UNIVERSITY OF TARTU
Faculty of Science and Technology
Institute of Technology

Seyedeh Elnaz Sadat Mansouri

A preclinical trial of Bisdemethoxycurcumin in a mouse model of Alzheimer's disease

Master's Thesis (30 ECTS)

Curriculum Bioengineering

Supervisor:

Associate Professor Miriam A. Hickey Ph.D.

Tartu 2022

A preclinical trial of Bisdemethoxycurcumin in a mouse model of Alzheimer's disease

Abstract:

Background: Alzheimer's disease (AD) is the most prevalent chronic neurodegenerative disease. The majority of currently approved therapies target symptoms of the disease and do not modify or prevent the disease's progression. Our past work and others have shown beneficial effects of curcumin on the neuropathology of AD models and models of other neurodegenerative diseases. Bisdemethoxycurcumin (BDMC) is another major curcuminoid found in spice turmeric, and here, we investigated nano-formulated bisdemethoxycurcumin (nBDMC), a novel therapeutic, in female wildtype and 5xFAD transgenic mice, which are a well-known model of AD.

Methods: Mice were administered with nBDMC over a two-month period from 6-7 to 8-9 months of age. Thioflavin S and Congo red stains were used to quantify amyloid levels and glial fibrillary acidic protein (GFAP) immunostaining was used to examine astrocytosis.

Results and conclusions: Amyloid quantification revealed no change in plaque load in frontal cortex or subiculum, and congo-red-stained plaque size was increased in frontal cortex. No change was observed in astrocytosis in the frontal cortex, caudal cortex, or subiculum. These data suggest that BDMC may not be an effective therapeutic for AD. In further work, we also examined endpoint pathology in untreated old 5xFAD mice (14m-old female wildtype and transgenic). At this age, body weights of transgenic mice were almost 40% less than their wildtype littermates and brain weights were 12% less. As expected for this model, plaque load was highest in subiculum followed by frontal cortex and then hippocampus. Despite this significant decrease in brain weight, no change in total hippocampal volume, the volume of hippocampal subregions or cortical volume was detected, which is consistent with previous work in these mice. However, in keeping with recent findings from patients with familial AD where reduced thalamic volume is more consistently observed than reduced hippocampal volume, we found reduced thalamic volume in our stereological analysis of 5xFAD mice, which carry five separate mutations that individually lead to AD in humans. These data reveal an important translational role of this mouse model for familial AD neuropathology.

Keywords:

Alzheimer disease, bisdemethoxycurcumin, neuropathology, 5xFAD

CERCS:

Neurology, neuropsychology, neurophysiology (B640)

Bisdemetoksükurkumiini prekliiniline uurimine kasutades Alzheimeri tõve hiiremudelit

Abstrakt:

Taust: Alzheimeri tõbi (AT) on üks kõige levinum krooniline neurodegeneratiivne haigus. Enamik praegu heakskiidetud ravimeetodeid on eelkõige sümptomaatilised ning ei mõjuta ega takista haiguse progresseerumist. Uuemad teadustulemused on kinnitanud kurkumiini kasulikku mõju nii AT loommudelite kui teiste neurodegeneratiivsete haiguste loommudelite neuropatoloogiale. Bisdemetoksükurkumiin (BDMC) on üks oluline kurkuminoid, mida vürtsikurkum sisaldab. Käesolevas töös viidi läbi uuring kasutades nanoformuleeritud bisdemetoksükurkumiini (nBDMC) - potentsiaalset uudset raviainet – emastel metsiktüüpi ja 5xFAD transgeensetel hiirtel, mis on hästi tuntud AT loommudel.

Meetodid: Töö käigus manustati hiirtele kahe kuu jooksul nBDMC-d, loomade vanusevahemik manustamise ajal oli 6–7 kuud kuni 8–9 kuud. Amüloidi taseme kvantifitseerimiseks kasutati tioflaviin S ja Kongo punase värvingut ning astrotsütoosi uurimiseks kasutati gliaalfibrillaarse happevalgu (GFAP) immunovärvingut.

Tulemused, Järeldused: Amüloidi kvantifitseerimine ei näidanud naastude ladestuse hulga muutust ei eesmises ajukoores ega subiculum´is ning Kongo-värvinguga punaseks värvunud amüloidnaastude suurus oli suurenenud eesmises ajukoores. Eesmises ajukoores, tagumises ajukoores ega subiculum´is astrotsütoosi muutusi ei täheldatud. Need andmed viitavad sellele, et nBDMC ei pruugi olla AT jaoks tõhus ravim.

Edasises töös uurisime ka lõpp-punkti patoloogiat vanadel 5xFAD hiirtel (14 kuu vanused emased metsiktüüpi ja transgeensed hiired). Selles vanuses oli transgeensete hiirte kehakaal peaaegu 40% väiksem kui nende metsiktüüpi pesakonnakaaslastel ja aju kaal oli vähenenud 12%. Nagu selle mudeli puhul eeldati, oli naastude ladestuse hulk suurim subiculum´is, millele järgnes eesmine ajukoor ja hipokampus. Vaatamata aju massi olulisele vähenemisele, ei tuvastatud hipokampuse koguruumala, hipokampuse alampiirkondade ruumala ega kortikaalse piirkonna ruumala muutust, mis on kooskõlas nendel hiirtel tehtud varasemate uuringutega. Siiski, võttes arvesse perekondliku AT-ga patsientidel teostatud hiljutiste uuringute leidudega, kus talamuse vähenemist täheldatakse järjepidevamalt kui hipokampuse vähenemist, leidsime 5xFAD hiirtel, kelle genoomi on sisse viidud viis perekondliku AT mutatsiooni, talamuse mahu vähenenemise. Need andmed näitavad selle hiiremudeli olulist translatsioonilist rolli perekondliku AT neuropatoloogia uurimisel.

Võtmesõnad:

Alzheimeri tõbi; bisdemetoksükurkumiin; neuropatoloogia; 5xFAD

CERCS:

Neuroloogia, neuropsühholoogia, neurofüsioloogia (B640)

TABLE OF CONTENTS

TERMS, ABBREVIATIONS AND NOTATIONS

AD - Alzheimer's disease

APOE - Apolipoprotein E

APP - amyloid precursor protein

FAD - familial Alzheimer's disease

PSEN1- presenilin 1

PSEN2 - presenilin 2

NFT - neurofibrillary tangles

SPs - senile plaques

Aβ - amyloid beta

MAP - microtubule-associated protein

ChE - cholinesterase

NMDA - non-competitive N-methyl-D-aspartate

BDMC - Bisdemethoxycurcumin

MTL - medial temporal lobe

5xFAD – a mouse model of AD that carries five familial AD mutations

GFAP - Glial fibrillary acidic protein

FAD - Familial Alzheimer disease

SAD - sporadic Alzheimer disease

BDMC - Bisdemethoxycurcumin

GWAS -genome-wide association studies.

MAF - minor allele frequency

OR - odds ratio

PRS - polygenic risk scores

INTRODUCTION

Alzheimer's disease (AD), the most common neurodegenerative disease, is characterized by cognitive and memory impairment caused by abnormal amyloid-beta deposition and hyperphosphorylated tau neurofibrillary tangles. Given the complexity of AD, treatment of patients remains challenging. At present, the majority of available therapies reduce symptoms and have little effect on neuropathology. Our past work and other studies have shown beneficial pharmacologic effects of Curcumin on neuropathology in mouse models of neurodegenerative disease (Hickey et al., 2012), and, in particular, in models of AD (Gagliardi et al., 2020). Curcumin is a naturally occurring spice from the rhizomes of turmeric plant. Several other bioactive polyphenols are present in these rhizomes, including bisdemethoxycurcumin. Despite its numerous neuroprotective effects, the use of curcumin is restricted due to its low water solubility, poor absorption, high metabolism, and poor permeability. To overcome this limitation, novel formulations and drug delivery technologies have been developed to improve brain delivery of curcuminoids, including nanoformulations that protect the drug and enhance its delivery to brain (Gagliardi et al., 2020). Bisdemethoxycurcumin (BDMC) is another major curcuminoid found in the spice turmeric and it shows high binding to amyloid in AD patient’s brains (Veldman et al., 2016a); however, its effects on amyloid pathology in vivo have not been examined thus far.

The 5xFAD mouse is a well-known transgenic model of AD, which carries five mutations associated with early-onset familial Alzheimer's disease (FAD): three mutations in the APP and two mutations in human presenilin-1(Oakley et al., 2006). It develops robust amyloid pathology from approximately 2 months of age, making it an ideal model for investigation of agents that may perturb amyloid formation. Our primary goal was to examine the effect of nano-formulated bisdemethoxycurcumin (nBDMC), a novel therapeutic, on plaques in the 5xFAD mouse model.

Despite the many studies completed on 5xFAD mice, end-stage pathology has not been fully described and indeed, consistent atrophy is not seen in hippocampus, the primary site of degeneration in patients with AD. Given that these mice carry mutation that causes familial AD, it is more likely that they mirror neuropathology of familial AD and not necessarily sporadic AD. We, therefore, set out to examine other sites of neurodegeneration that have been recently described in familial AD. Thus, an additional goal was to investigate endpoint pathology in untreated elderly 5xFAD animals.

1 LITERATURE REVIEW

1.1 Alzheimer's Disease

Alzheimer's disease (AD), the leading cause of dementia in the elderly, is a progressive neurodegenerative disorder that progresses to cognitive impairment and dysfunctions in complex daily activities and subsequently leads to death (Kukull & Bowen, 2002).

The neuropathological features of Alzheimer's disease include the aggregation of the abnormal proteins amyloid-β, in plaques, and hyperphosphorylated-tau, in neurofibrillary tangles. These aggregates lead to massive loss of synapses, dendrites, and eventually neurons in the brain of AD patients. The actual causes of Alzheimer's disease are still not well defined; however, age is the most potent risk factor, followed by the ε4 allele of apolipoprotein E (APOE ε4), and cardiovascular, e.g., increased blood glucose, and lifestyle risk factors. Notably, frequent exercise, mental activity, a healthy lifestyle, and a healthy diet reduce the risk of dementia, particularly Alzheimer's disease (Jha & Mukhopadhaya, 2021).

The severity of cognitive impairment in AD increases with advancing age and may be scored with tools such as the MiniMental State Exam (Tombaugh et al., 1996). However, when patients are grouped based upon the age of onset, about 5% develop symptoms before the age of 65 and are termed "patients with early-onset Alzheimer's disease" (EOAD). The majority of patients develop their symptoms after 65 and are termed "late-onset Alzheimer's disease" (LOAD)(Awada, 2015).

1.2 Genetics

Genetically, AD cases may be categorized as familial or sporadic (Piaceri et al., 2013). Rare autosomal dominant mutations in three genes, *amyloid precursor protein* gene on chromosome 21, *presenilin 1* gene on chromosome 14, and *presenilin 2* gene on chromosome 1, cause familial Alzheimer's disease. These mutations are identified as predictive factors for the development of AD (Zhang et al., 2020).

Many genetic and environmental variables contribute to sporadic Alzheimer's disease, but the most critical risk factor is the apolipoprotein E gene on chromosome 19, with three main alleles including ε2, ε3, and ε4. APOE gene is a lipoprotein that helps carry cholesterol, lipid, and other types of fat in the bloodstream. Type 3 and 4 alleles of this gene is observed in more than 50 percent of patients with AD. Type ε 4 alleles can increase the risk of AD with homozygotes carrying the highest risk and greatest amyloid load, and indeed, memory impairment is strongest in homozygote ε-4-allele carriers (Jansen et al., 2015).

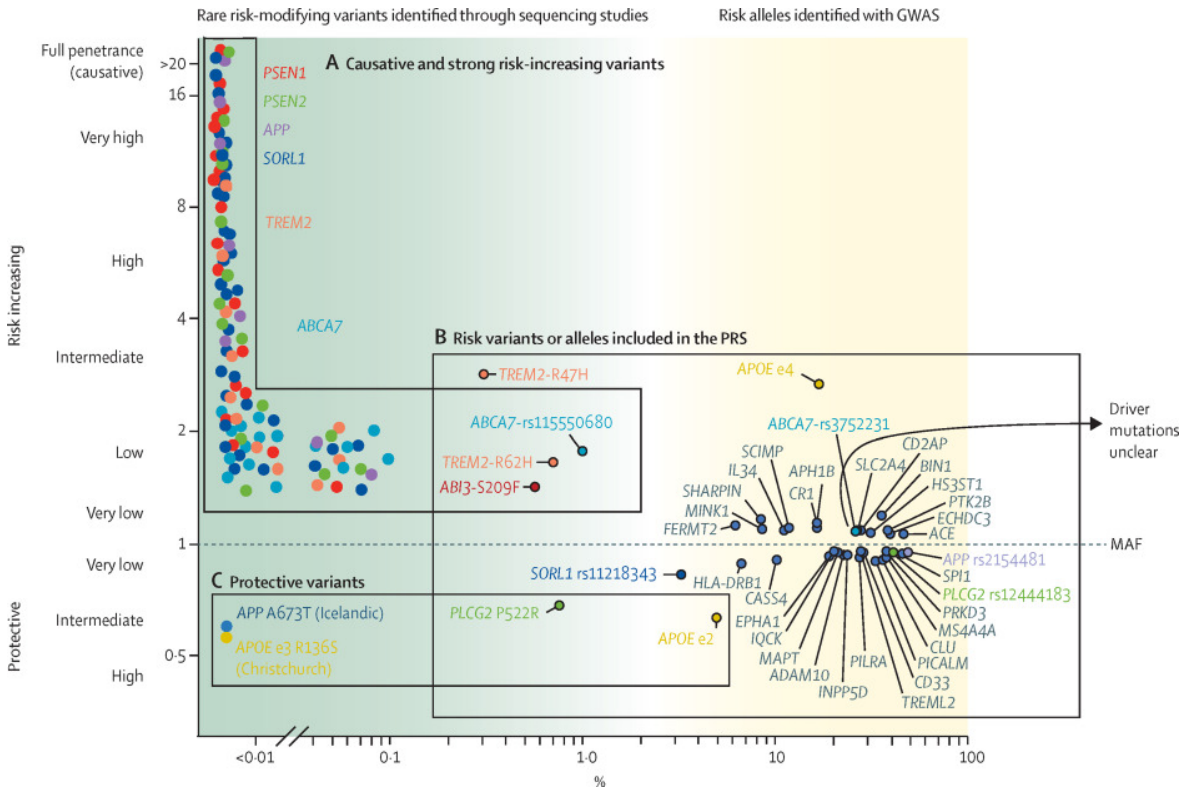

Figure 1. The genetic overview of Alzheimer's disease. the x-axis shows the frequency of variant alleles, and the y-axis shows the odds ratio of developing Alzheimer's disease. (A) three rare variants in PSEN1, PSEN2, and APP cause autosomal dominant Alzheimer's disease, and variants in the SORL1, ABCA7, and TREM2 genes were also found with inheritance patterns of autosomal dominant inheritance. (B) GWAS hits are risk alleles that occur with significantly different frequency in patients with Alzheimer's disease and controls. The gene represents each variant. (C) Protective variants give resistance against age-associated or disease-associated risk factors of cognitive decline (Scheltens et al., 2021)

1.3 Clinical manifestations

Alzheimer's disease includes early and progressive episodic memory defects that often remain in later stages and are associated with other cognitive disorders. Deficits include Amnesia (memory loss), Aphasia (difficulty in finding words and speaking), Apraxia (inability to complete taught motions), Agnosia (failure to interpret sensory input correctly), and Abnormal executive function (planning, insight, judgment) (Jha & Mukhopadhaya, 2021).

The degree of cognitive impairment in AD significantly affects the patient's desires and abilities to interact in activities. A preclinical phase is characterized by the early onset of amyloid deposition and early neuroinflammatory changes. This is followed by the spread of neurofibrillary tangle (NFT), synaptic dysfunction and synapse loss. Onset and progression of cognitive impairment correlate with accumulation of AB, tau, and hippocampal volume loss. Diagnosing Alzheimer's disease requires identifying the clinical symptoms and eliminating frequent causes of dementia in the elderly. The Clinical Dementia Rating (CDR) scale can be used to stage AD, with a score of 0 indicating normal cognition and scores of

0.5, 1, 2, and 3 indicating questionable, mild, moderate, and severe dementia (Zhang et al., 2020).

In the early stages, patients become forgetful, they frequently lose items, and they have difficulties communicating, choosing the right words, and making decisions. Other symptoms include memory loss, confusion, and the inability to recall familiar individuals or locations. In the middle stage, depression and anxiety are visible. People become highly forgetful, have difficulties understanding time, dates, places, and events, require assistance with personal care, and cannot live alone safely without significant support. In the final stage, patients are almost totally dependent and immobile (Jha & Mukhopadhaya, 2021).

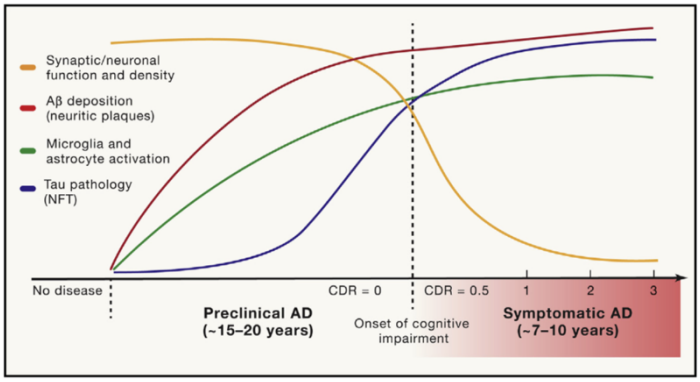

Figure 2. Pathophysiological events in Alzheimer's Disease concerning Clinical Progression. The Clinical Dementia Rating (CDR) scale can be used to stage the onset and severity of clinical symptoms, with a score of 0 indicating normal cognition and scores of 0.5, 1, 2, and 3 indicating doubtful, mild, moderate, and severe dementia, respectively, (Long & Holtzman, 2019a).

1.4 Pathophysiology of AD

The brain of an Alzheimer's patient undergoes several molecular and cellular alterations. Alzheimer disease is characterized by brain atrophy, neuro-inflammation and vascular changes, and many changes are observed in brain prior to diagnosis (Figure 2). The most important pathological markers are deposits of two abnormal proteins, namely Extracellular Amyloid Plaques and intracellular Neurofibrillary tangles (Scheltens et al., 2021).

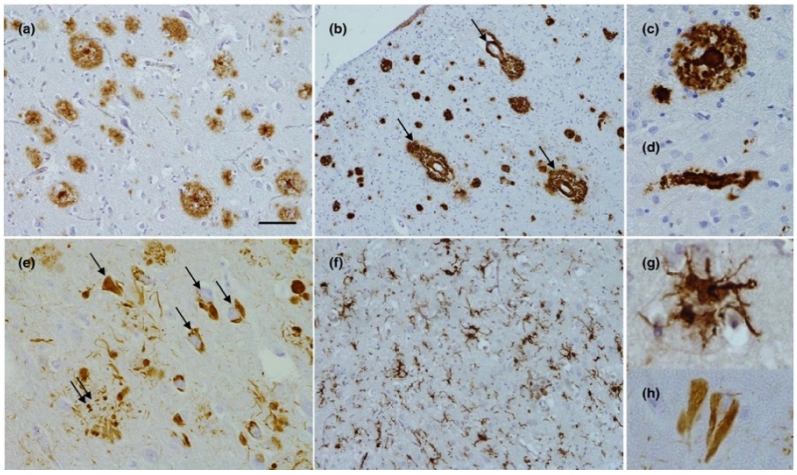

Figure. 3 Pathology of AD. Aβ immunohistochemistry shows the plaques in the frontal cortex (a) and cerebral amyloid angiopathy (b), shown at greater magnification (c). Aβ accumulates within capillaries in severe cerebral amyloid angiopathy (d). Tau immunohistochemistry shows neurofibrillary tangles (e, arrows; h at higher magnification) as well as neuritic plaques (e, double arrow). The quantity of activated microglia demonstrates that neuroinflammation is a critical component of Alzheimer's disease (f; g at higher magnification). The bar represents 50 μm in a and f; 100 μm in b; 25 μm in c and e; 15 μm in d, g and h (Lane et al., 2018)

1.4.1 Amyloid hypothesis

The amyloid hypothesis of Alzheimer's disease suggests that deposition of the amyloid-β peptide in the brain is a significant cause of Alzheimer's disease. Aβ is made following sequential cleavage of APP (a single transmembrane protein that is enriched in neuronal synapses) by 2 enzymes: β-secretase, and γ-secretase, through the amyloidogenic pathway (Long & Holtzman, 2019).

The β-secretase enzyme (BACE1) cleaves APP at the N terminus of the Aβ sequence. Presenilin (PSEN), presenilin enhancer (PEN), APH, and Nicastrin are the four protein components of the γ-secretase complex. Following cleavage by BACE1, the γ-secretase complex binds to N-terminally cleaved APP fragment and cleaves at the ε-site, releasing C-terminal fragment and Aβ48. The γ-secretase complex then proceeds along the remaining Aβ C-terminal end, creating shorter peptides until the Aβ peptide is released from the complex (Long & Holtzman, 2019). The amyloid plaques are generated from soluble monomers, dimers, oligomers, and insoluble fibrils. The significant components of accumulated Aβ are Aβ 40 and Aβ 42, containing 40 and 42 amino acids, respectively. Mutations in APP and presenilin that increase Aβ production are strongly linked to disease. In the absence of Aβ amyloid deposition, synaptic deficits and dendritic dysplasia occur (Long & Holtzman, 2019). During the five Thal stages, Aβ peptide deposits move from the neocortex to the entorhinal region and the hippocampus, eventually reaching the subcortical

structures, the brain stem, and the cerebellum (Jouanne et al., 2017). Importantly, Aβ pathology may be observed in brains of individuals with preclinical AD, and the extent of Aβ pathology changes relatively little during the course of the symptomatic stages of the disease (van der Kant et al., 2020).

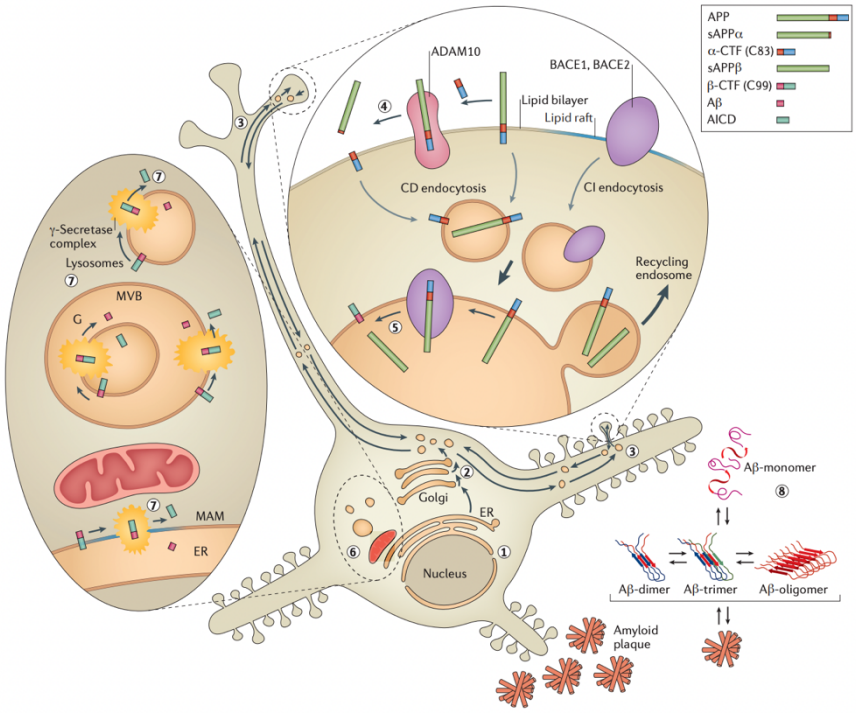

Figure 4. Pathways of amyloid precursor protein. In brief (not all steps covered), amyloid precursor protein is produced and processed in the endoplasmic reticulum (step 1). It is modified post-translationally in the ER and then in the Golgi (step 2). The modified APP is then transported into presynaptic and postsynaptic compartments (step 3). In the case of non-amyloidogenic processing, APP is cleaved to generate soluble APPα and α-secretase C-terminal fragments (step 4). APP, BACE1, and BACE2 converge in early endosomes, and the low pH of these compartments enables the activation of these β-secretases, and the initiation of the amyloidogenic pathway where APP is cleaved into soluble APPβ and β-secretase C-terminal fragments. The final γ-cleavage of APP takes place in mitochondria-associated ER membranes, MVBs, and lysosomes (step 7). There, β-CTF is recognized by the γ-secretase complex and cleaved to generate the APP intracellular domain and amyloid β peptides. In the formation of amyloid plaques, Aβ monomers exist in equilibrium with higher-molecular-mass aggregates (dimers, trimers, and oligomers) (step 8)(Polanco et al., 2018)).

1.4.2 Tau hypothesis

Tau protein controls tubulin assembly durability and the tau gene (on chromosome 17). The amyloid hypothesis suggests that amyloid instigates neuropathology in AD; however, according to the tau hypothesis, tau tangle pathology occurs before Aβ plaque development. NFTs, also known as tangles, are intraneuronal protein aggregates made mostly of paired helical filaments of the hyperphosphorylated microtubule-associated protein tau (Myers & McGonigle, 2019).

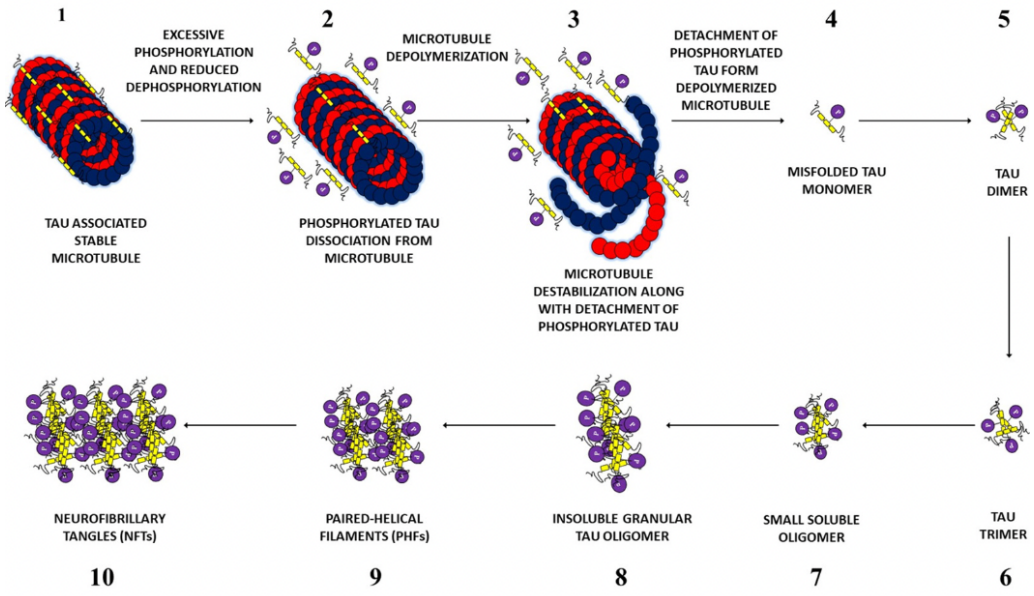

Figure 5. Sequential steps in NFTs formation. Before neurofibrillary tangle (NFT) formation, tau aggregates and forms tau monomer, dimer, trimer, oligomer, granular tau oligomer, and filament. Hyperphosphorylated tau and tau oligomers are involved in synapse loss, and granular tau oligomer causes neuronal loss (Muralidar et al., 2020).

Tau has a strong relationship with the severity of cognitive and clinical symptoms (Kametani & Hasegawa, 2018). It is associated with grey matter shrinkage and cognitive impairment. Tau pathology is first observed in the entorhinal cortex, and from there it spreads to limbic areas and to cortex during the progression from presymptomatic to mild cognitive impairment and to AD dementia (van der Kant et al., 2020). However, these more simplistic models have been challenged in recent years (Frisoni et al., 2022).

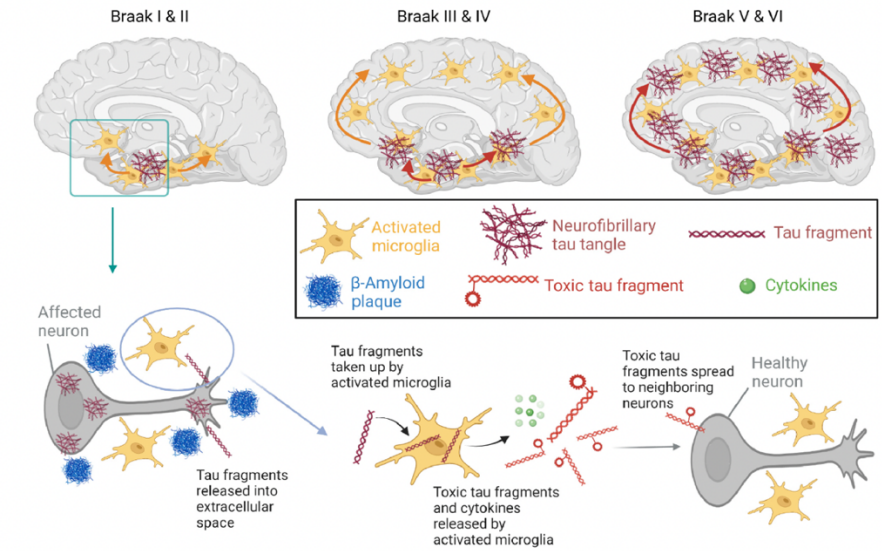

Figure 6. Propagation of Tau pathology. Tau pathology starts in the medial temporal cortex and then spreads. Microglial activation may indeed precede and potentiate the spread of tau (top panel). When β -amyloid is present, intracellular tau is released into the extracellular region and phagocytosed by microglia (bottom panel) (Rossano & Kreisl, 2021).

1.4.3 Neuroinflammation in AD

Alzheimer's disease pathogenesis is strongly associated with immunological mechanisms in the brain. Misfolded and aggregated proteins interact with pattern recognition receptors on microglia and astrocytes, triggering an innate immunity defined by releasing inflammatory mediators that contribute to disease development and severity (Heneka et al., 2015).

Neuroinflammation is a feature of Alzheimer's disease and is defined by the clustering of reactive astrocytes and microglia around Aβ plaques and upregulated levels of pro inflammatory mediators (Oakley et al., 2006).

1.4.3.1 Microglia

Microglia are the resident immune cells within the central nervous system. Microglia are in an inactive, "resting" state in a healthy brain. When microglia identify to threat the CNS, such as invasion, injury, or disease, they become activated, causing a morphological change resulting in retraction of processes, enlargement of the cell, and migration. The presence of Aβ is the major activator of microglia. Activated microglia respond to Aβ by migrating to the plaques and phagocytosing Aβ (Leng & Edison, 2021).

1.4.3.2 Astrocytes

Astrocytes are specialized glial cells that form the entire CNS scaffold and can be found in protoplasmic or fibrous form. Astrocytes control cerebral blood flow, maintain fluid homeostasis and neurotransmitter levels, initiate synapse development, and offer metabolic and neurotrophic support for synapses. Astrocytes also generate glyphosate-resistant perivascular canals in the CNS, known as the glyphosate system. Amyloid-containing granules in astrocytes have been seen around amyloid plaques in the human brain, indicating that astrocytes try to remove amyloid deposition during the disease process. In vitro, astrocytes move to amyloid plaques and destroy Aβ and collaborate with microglia and can help minimize some of the harmful consequences (Leng & Edison, 2021). However, A1 astrocytes, which are toxic to the CNS, are prevalent in brain tissue after death in persons with Alzheimer's disease, suggesting that these cells have a negative function.

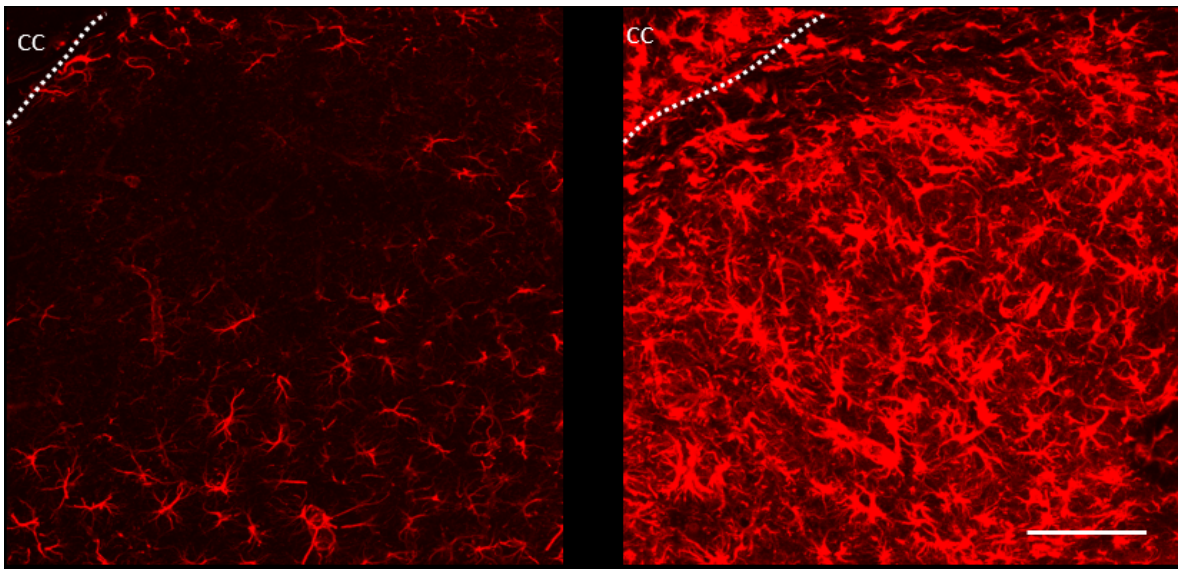

Figure 6. Astrocytes in the 5xFAD mouse model of AD. Wildtype (left) and transgenic 5xFAD (right) subiculum from 6-month-old mice stained using an anti-GFAP antibody. The dashed line shows the border of the subiculum with the corpus callosum. Sagittal sections, approximately -3mm from bregma. The bar represents 100 μm for both left and right (adapted from Hickey lab).

1.5 Therapy

Alzheimer's disease therapy options are currently being researched extensively. In clinical trials, both Aβ and tau are important targets for disease-modifying therapies (DMTs) in AD. According to this viewpoint, AD might be prevented or effectively treated by decreasing the production of Aβ and/or tau; preventing aggregation or misfolding of these proteins; neutralizing or removing the toxic aggregated or misfolded forms of these proteins, or a combination of these modalities (Yiannopoulou & Papageorgiou, 2020).

Despite numerous attempts to develop novel therapeutic methods to prevent disease development, only one anti-Aβ medications has been developed by far, and even this is controversial (Walsh et al., 2021). The Alzheimer's drug pipeline remains full of agents with mechanisms of action (MOA) targeting disease modification or symptoms. The most popular and broadly accepted explanations for the multiple failures of clinical trials of DMT agents for AD are that therapies begin too late during disease development, inappropriate drug doses, incorrect targeting, and an inadequate understanding of the pathophysiology of AD (Hampel et al., 2018).

The majority of currently available therapies attempt to correct the disease's neurotransmitter imbalance (Yiannopoulou & Papageorgiou, 2020). They are the cholinesterase inhibitors (donepezil, rivastigmine, and galantamine) and the N-methyl-D-aspartate (NMDA) receptor antagonist memantine. Donepezil and rivastigmine have been approved by FDA for mild, moderate, and severe AD, whereas galantamine for mild and moderate AD. However, the mechanisms of action of the cholinesterase inhibitors cause negative effects in the periphery,

including nausea, vomiting, loose stools or loss of appetite, muscle cramps, headaches, and bradycardia. Neither cholinesterase inhibitors nor memantine affects the underlying biology of Alzheimer's disease (Knopman et al., 2021). Moreover, the duration of efficacy is limited to 6 months or less (Bishara et al., 2015).

Growing evidence shows a protective effect of Curcumin against Aβ plaque formation; however, the mechanism of action is not yet fully clarified (lo Cascio et al., 2021). Curcumin's bioavailability is restricted, and it has yet to be shown to be effective in patients (Congdon & Sigurdsson, 2018).

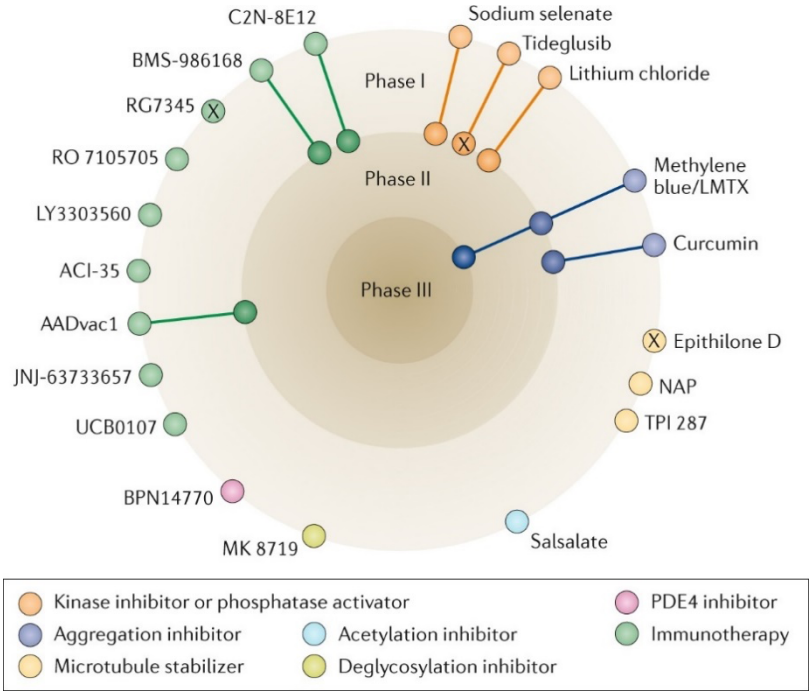

Figure. 7: Status of clinical trials of drugs that target tau pathology. The most active field is tau immunotherapy, with two active vaccines (AADvac1 and ACI-35) and six antibodies (LY3303560, RO 7105705, BMS-986168, C2N-8E12, JNJ-63733657 and UCB0107) in clinical trials (Congdon & Sigurdsson, 2018b).

1.5.1 Properties of Curcumin

Curcumin is a diferuloylmethane polyphenol with two phenolic rings. Curcumin is an active molecule found in the turmeric root and has been widely used for medicinal purposes for years as a traditional Indian and Asian medicine. It has well-known anti-cancer and hypoglycaemic characteristics and the possibility to be used as an analgesic, antibacterial, or antimalarial. It has been shown to have anti-inflammatory, antioxidant, and anti-amyloidogenic properties, which are relevant for treating Alzheimer's disease (lo Cascio et al., 2021b). Curcumin has an inhibitory effect on NFκB, which plays a pivotal role in the

inflammatory response, thereby reducing inflammation (Gagliardi et al., 2020). It acts through several mechanisms and prevents the formation of β-amyloid, tau and may reduce microglial density (Ege, 2021).

Curcumin is consumed by millions of people every day, and it is completely safe for both animals and humans (Gagliardi et al., 2020). Little toxicity has been found in animal models. Similarly, few adverse effects of Curcumin have been observed in humans even at extremely high dosages (Sharma et al., 2005).

Curcumin's lipophilic nature makes it challenging to formulate into a therapeutic product. Oral administration is the most convenient way of medicine administration, followed by enteral absorption. Curcumin is extensively metabolized during first-pass metabolism, resulting in low bioavailability. Even when injected intraperitoneally to avoid the gut, Curcumin has metabolized in the liver via Phase II mechanisms (Gagliardi et al., 2020).

Curcumin and other curcuminoids have been shown to bind directly to AD plaques in humans (Veldman et al., 2016b) and in mice (Maiti et al., 2016). Curcumin significantly reduces the amounts of intracellular oligomers and prefibrillar production in of several aggregating proteins, including huntingtin (Hickey et al., 2012), with doses at manageable levels. Curcumin is well known to inhibit β-fibril growth by reducing antiparallel beta-sheet secondary structures inside Aβ oligomers and without affecting monomer interactions. (Yang et al., 2005). Curcumin alters fibrillar architecture and reduces both soluble and insoluble Aβ. It reduces the rate at which Aβ is induced into anionic membrane lipids and slows APP maturation in the secretory pathway. Curcumin's anti-amyloid action may also be attributed to increased soluble oligomers of Aβ rather than prevention of fibril formation. (Yang et al., 2005). Curcumin has been shown to decrease BACE-1 overexpression, (Zheng et al., 2017) reducing amyloid aggregates and altering AD pathogenesis. Curcumin therapy can decrease PS1 expression, decreasing γ-secretase and, as a result, indirectly attenuate A40/42 aggregation (Radbakhsh et al., 2021).

Therefore, Curcumin has been recommended as a potential treatment method for Alzheimer's disease in several preclinical trials; however, efficacy has been limited (Gagliardi et al., 2020). The low bioavailability of Curcumin after oral administration and its fast metabolism hampers its use and necessitates the use of formulations that protect it. As a result, novel formulations and drug delivery technologies, including as liposomes and nano-based techniques, have been developed to improve curcumin brain delivery. In a mouse model, Curcumin with nano-capsules show a considerably stronger neuroprotective impact against AB toxicity rather than free Curcumin (Gagliardi et al., 2020).

1.5.2 New Formulations and increased the bioavailability of Curcumin

Bisdemethoxycurcumin (BDMC) is a constituent of turmeric that is more stable than the other two constituents curcumin and desmethoxycurcumin (di Meo et al., 2019) .However, despite promising data suggesting that BDMC binds plaques in patient tissue, little in vivo research has been undertaken with this molecule (Veldman et al., 2016b).

Our collaborators designed a methodology for encapsulating BDMC within H-ferritin nanocages (Pandolfi et al., 2017). H-ferritin nanoparticles interact with the trans ferritin receptor, which is abundant on the luminal surface of endothelial cells, and they are subsequently transcytosed across the blood-brain barrier (Shahryari et al., 2016).

1.6 Mouse Model

Animal models have been a significant priority in preclinical studies in AD pathophysiology and to predict outcomes from pharmacological treatment (Webster et al., 2014). However, it must be noted that despite many articles on preclinical investigations in AD mouse models, trial designs remain inadequately powered (Gagliardi et al., 2020)

They can be used to evaluate the disease at the early level and investigate the role of individual genes and disease mechanisms in neurodegeneration (Elder et al., 2010).The majority of available mouse models were developed based on risk factors and pathology discovered in human studies. Although none are perfect, each has benefits as well as drawbacks (Tai et al., 2021).

AD is an ideal disease for modelling in transgenic animals due to a well-known pathology consisting of senile plaques and NFT and other pathological features include neuronal and synaptic loss, dystrophic neuritis, active astrocytes, and active microglia. Also, a well-defined behavioral phenotype can be modelled in mice. Most AD mice models represent the familial form of AD (FAD), which accounts for just a small percentage of overall AD cases annually (Webster et al., 2014). To model sporadic AD forms, only some mice would develop AD and only at advanced ages (Tai et al., 2021).

Table 1. commonly used mouse models of AD

Name	Genetics	Neuropathology	Behavioural deficits	year	Reference
PADAPP	hAPP (Ind), human PDGF-β promoter, C57BL/66 × DBA2	Aβ plaques by 6-8 months, no tau pathology, gliosis, CAA	Spatial memory by 3 months	1995	Games et al. (1995); Rockenstein et al. (1995)
Tg2576	hAPP (Swe), isoform 695; hamster PrP promoter; B6/SJL mixed background	Aβ plaques by 9-11 months, no tau pathology, gliosis, synaptic loss, CAA	Spatial and learning memory by 6 months	1996	Hsiao et al. (1996)
APP23	hAPP (Swe), isoform 751; mouse Thy1 promoter; C57BL/6	Aβ plaques by 6-8 months, hyperphosphorylated tau but no tangles, gliosis and neuronal loss, CAA	Progressive in recognition and spatial memory by 3 months	1997	Sturchler-Pierrat et al. (1997)
APPPS1/PS1	m/hAPP (Swe), hPSEN1 (□E9), mouse PrP promoters, (C57BL/6 × C3H)F2	Aβ plaques by 6-9 months, no tau pathology, gliosis, synaptic and neuronal loss, CAA	Spatial and reference memory by 6 months	1998	Jankowsky et al. (2004)
J20	hAPP (Swe, Ind), human PDGF-β promoter, C57BL/6	Aβ plaques by 6-8 months, no tau pathology, gliosis, synaptic and neuronal loss, CAA	Recognition memory by 2 months and spatial memory by 3 months	2000	Mucke et al. (2000)
APPPS1	hAPP (Swe), hPSEN1 (L166P), mouse Thy1 promoter, C57BL/6J	Aβ plaques by 6-8 months, no tau pathology, gliosis, synaptic and neuronal loss, CAA	Spatial and memory by learning 7 months	2001	Radde et al. (2006)
TgCRNS8	hAPP (Swe, Ind), hamster PrP promoter, hybrid C3H/He-C57BL/6	Aβ plaques by 3-5 months, no tau pathology, gliosis, synaptic and neuronal loss, CAA	Progressive in working and spatial memory by 6 months	2001	Chishti et al. (2001)
3Tg	hAPP (Swe), hPSEN1 (M146V), hMAPT (h0N4R P301L), mouse Thy1.2 promoter (APP, MAPT), endogenous PSEN1 promoter, C7BL/6;129X1/ SvJ;129S1/Sv	Aβ plaques by 6 months, tau pathology by 12 months, gliosis	Progressive in learning memory by 4 months and spatial memory by 6 months	2003	Oddo et al. (2003)
5FAD	hAPP (Swe, Fl, Lon), hPSEN1 (M146L, L286V), mouse Thy1 promoter, C57BL/6 × SJL	Aβ plaques by 2 months, no tau pathology, gliosis, synaptic and neuronal loss, CAA	Progressive in spatial memory by 3 months and learning memory by 6 months	2006	Oakley et al. (2006)

1.6.1 5XFAD mouse model

The 5xFAD mouse is a transgenic model of AD carrying five mutations associated with early onset familial Alzheimer's disease (FAD): three in the APP695 gene [APP K670N/M671L (Swedish), I716V (Florida), and V717I (London) mutations in human amyloid precursor protein (APP) and two genes including the M146L and L286V mutations in human presenilin-1 (Oakley et al., 2006).

The Swedish mutation enhances overall Aβ production, but the APP Florida and London mutations and the PS1 gene exclusively boost Aβ42 production (Oakley et al., 2006).

1.6.2 5XFAD Neuropathology

Plaques first develop by approximately 2m of age in subiculum and deep layers of the cortex. Amyloid deposits progress in size and density and spread to the greater hippocampus to layer V of the cortex and greater hippocampus with age. In recent years, more fine analysis has revealed ever more detail, with mammillary body, septum, and subiculum being most affected at early stages (2m) (Gail Canter et al., 2019).

The 5XFAD also develop extensive neuroinflammation (astrogliosis and microgliosis). Neuronal loss in cortical layer 5 develops by approximately 9 months (Eimer & Vassar, 2013). 5XFAD have not been thought to develop abnormally phosphorylated tau epitopes; however, more recent data suggests that they do (Mattsson-Carlgren et al., 2020). Although early work suggested that cognitive deficits were present from approximately 4 m (Oakley et al., 2006), recent data, using balanced, larger groups suggests no serious cognitive deficits and that indeed, motor hyperactivity is the most robust finding (Oblak et al., 2021). Clearly, even though these mice are well-used, they have much yet to reveal.

2 THE AIMS OF THE THESIS

In this study, we used brain tissue from the 5xFAD mouse model of Alzheimer's disease to investigate neuropathological effects of a novel therapeutic.

In this study, the specific aims are:

- to investigate the effects of nano formulated Bisdemethoxycurcumin on amyloid plaques and neuroinflammation in 8-9month old 5xFAD mice, a model of Alzheimer's disease.
- to examine end-stage pathology in 5xFAD mice at 13-14 months of age.

3 EXPERIMENTAL PART

3.1 MATERIALS AND METHODS

3.1.1 Animals

Wild type and transgenic female 5XFAD mice were used (MMRRC stock number #34840; background: B6SJLF1) (Oakley et al., 2006).

For the preclinical study, 6-7-month-old female 5xFAD mice (N=16 WT; N=12 TG control; N=12 TG treated) were treated twice weekly for 2 months with intraperitoneal injections of 1mg/kg nanoformulated BDMC, diluted in sterile physiological saline (dose-volume 0.1ml/kg). Control mice were treated with sterile physiological saline. At 8–9-months of age, mice were euthanised. Behaviour was examined but is not discussed here.

In the Endpoint study, female WT (N=6) and TG (N=6) mice were euthanised at 13-14 months of age, when TG mice weight less than 50% of WTs.

At euthanasia, brains of mice were dissected out and placed in fresh 4% paraformaldehyde and incubated at 4°C for 2-3 days. They were then cryoprotected in 30% sucrose in 0.01M PBS for 2 days and then frozen in liquid nitrogen. Brains were stored at -80°C until processing. The brains were coronally sectioned at 40 microns section thickness from approximately -4.6mm AP to approximately +2mm AP.

Mice had free access to food and water in standard laboratory conditions, and the light cycle was 12 hours on, 12 hours off. All experiments with animals were performed in accordance with the EU Directive 2010/63/EU US and were approved by the Estonian Ministry of Rural Affairs (licences 140 and 175). The mice were handled by Dr MA Hickey and her staff who are authorized to perform this work.

All analyses were conducted blinded.

3.1.2 Staining

3.1.2.1 Congo red and Cresyl Violet

Serial coronal sections (1:10) were picked from approximately +1.7mm to -4.5mm relative to bregma (cortex + hippocampus) for the preclinical trial and from approximately -1mm to -4.5mm (hippocampus) for the Endpoint cohort. Briefly, the first section of the stereological series was chosen at random from the first 10 sections of the region of interest, to eliminate bias. Every 10^{th} section thereafter was chosen such that 400 µm was the advance between each section. Sections were stored in cryoprotectant until processing. Sections were washed

in PBS for 3x5 minutes on the rotator. They were rewashed three times in 0.01M TB and then mounted on gelatin-coated glass slides. After drying completely, sections were stained according to the following protocol for Congo red and Cresyl Violet staining: sections were rinsed in distilled water for 30 seconds, then dehydrated through 80% ethanol and 1M NaCl for 20 minutes. Sections were stained using 0.2% congo red in saturated NaCl (Feng & Shoi-chet, 2006).for 30 minutes and then rinsed in distilled water to remove any residual salts for 2 minutes. Slides were then placed in cresyl violet (Acros Organics, 0.2g in 150ml dH2O) for 10 minutes and rinsed in tap water to remove any excess stain. Slides were then dehydrated through 70% ethanol once and three times in 96% ethanol, cleared in xylene replacement for 3x3minutes and then coverslipped using a mounting medium (Eukitt).

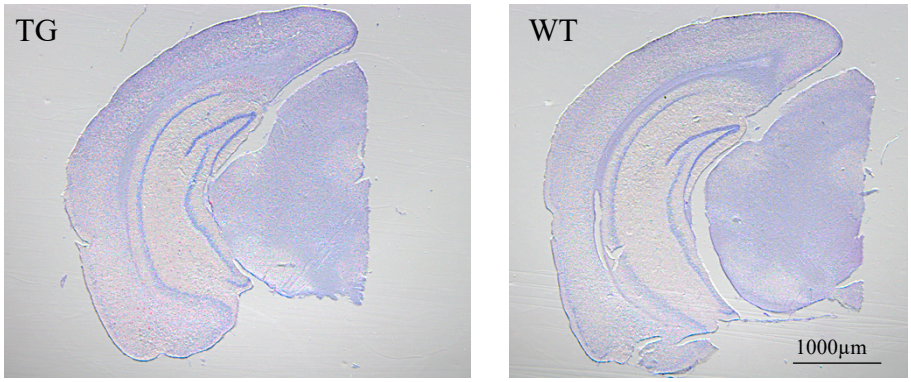

Figure 8. Staining of coronal section of brain tissue with Congo red and Cresyl Violet. Both images show results for CR and CV staining in Endpoint cohort (note CR staining in subiculum in TG mouse). Images were taken at x34 magnification.

For the preclinical trial, hippocampus and overlying cortex images were taken with stereomicroscope 40x magnification (Zeiss Axio imager, Zen software (2010)). For volume analysis for the Endpoint cohort, images were taken with a stereomicroscope (Zeiss Axio imager, Zen software (2010)) for 1) Cortex at 17x magnification (Zeiss Axio imager), 2) Hippocampus (DG, CA1, CA2 and CA3) and SUB at 34x magnification (Zeiss Axio imager) and 3) for Thalamus using Odyssey M (LI-COR) Imaging System to cover the whole of the thalamus.

All images were then processed within Fiji Image J (W. Rasband, USA, version 2.3./1.53q).

3.1.2.1 Thioflavin S

For staining with thioflavin-S (TF-S), four coronal sections (two rostral sections at approximately +0.62mm Bregma and two caudal sections at approximately -3.68mm relative to Bregma) were used for the Preclinical trial (40 mice) and the End stage cohort (12 mice).

Sections were washed in 0.01 M PBS for 3x5 min and then rewashed three times in 0.01M TB for 5 min on the rotator. The sections were mounted onto gelatin-coated glass slides.

The slides were washed quickly three times in tap water, and then they were stained with TF-S and incubated for 30 min (1% w/v). The sections were then dehydrated in 70%, 96%, and 96% ethanol for 5 minutes each, followed by defatting for 3 x 5minutes in xylene replacement. They were mounted in a mounting medium (Eukitt) and stored in the dark before examination by fluorescence stereoscopy. Imaging was performed using a stereomicroscope (Zeiss Axio imager) at x40 magnification for the Endpoint cohort and x27 magnification for preclinical cohorts. Images were stitched using Auto-Stitch (http://matthewalunbrown.com/autostitch/autostitch.html). Amyloid was measured using Fiji Image J (W. Rasband, USA, version 2.3./1.53q).

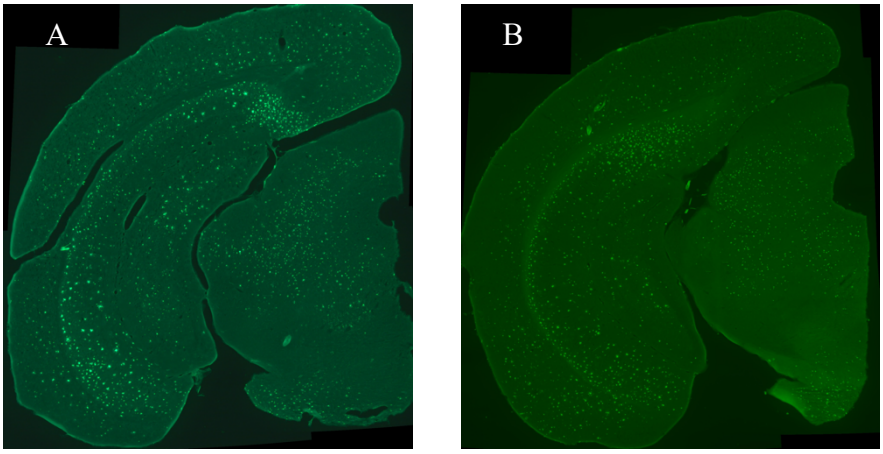

Figure 9. Representative staining of coronal sections with Thioflavin S. (A) shows a representative image from the end-stage trial result. (B) Shows a representative image from the preclinical trial.

3.1.2.2 Immunofluorescence

For immunostaining, two sections at approximately +1.5 mm relative to Bregma and two sections at approximately -3mm relative to Bregma were picked from each of 40 mice from the preclinical trial. Two sections were picked from one mouse and used as control samples as they were not exposed to the primary antibody. Sections were washed in PBS for 3x5 minutes on the rotator. Sections were then blocked for 30 minutes using 5% goat serum in 0.5% Triton X in PBS. They were then incubated overnight with rabbit polyclonal to GFAP antibody (HPA056030, Merck; 1:500 dilution). The following day, sections were again washed for 3x5min in 0.0M PBS, followed by a 2-hr incubation in goat anti-rabbit secondary antibody (111-585-003, JacksonImmunoResearch; 1:500 dilution). After washing with 0.01M PBS, the sections were incubated in Hoechst (1µg/ml) for 10 minutes. Finally, they were rewashed three times in 0.01M TB and then mounted on gelatin-coated glass slides

with fluorescence mounting medium (made in-house). The slides were stored flat at -20°C until imaging. Imaging of astrocytes (two sections at approximately +1.145mm Bregma and two sections at approximately -3.38mm Bregma) was taken with a confocal microscope (Zeiss LSM780) using Zen software (2010). We obtained our images ~20 µm below the brain surface. All pictures were taken at the same settings (x10 magnification, 1.42mm x 1.42mm image size at 1024 x 1024 pixels; GFAP: ex 561nm, em 659nm; Hoechst: ex 405nm, em 495nm) to ensure consistency.

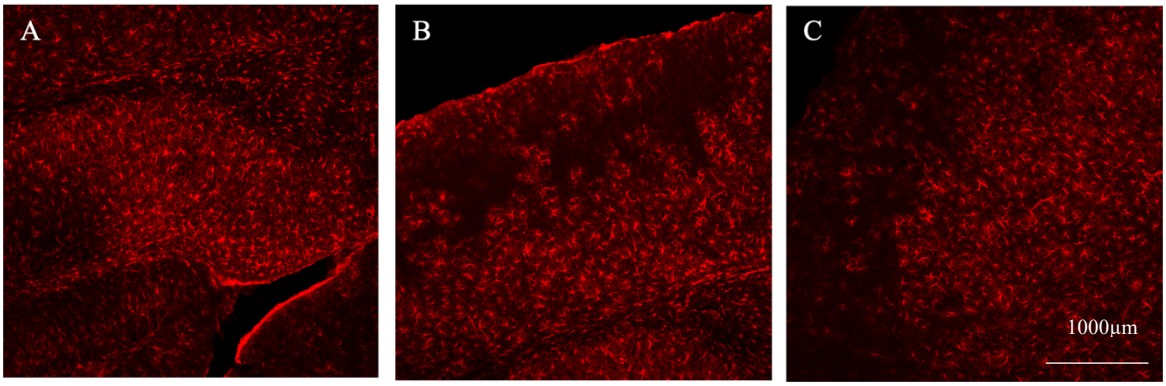

Figure 10. Representative immunostaining for GFAP in coronal sections from the preclinical trial. (A) subiculum, bregma -3.38mm. (B) Visual cortex overlying subiculum, Bregma -3.38mm. (C) Frontal somatosensory cortex, Bregma 1.145mm. Scalebar x10. Note: For analysis, the subiculum was outlined based upon Hoechst staining (taken at the same time as the GFAP image but not shown here) and this ROI was then placed on GFAP image for analysis. For the visual cortex, the cortex was outlined based upon Hoechst staining (taken at the same time as the GFAP image but not shown here) and then the ROI was placed upon the GFAP image for analysis. The entire frontal cortex was analysed.

3.1.3 Data Analysis

All data analysis was performed with Fiji ImageJ Software (W. Rasband, USA, version 2.3./1.53q), the most up-to-date version of data quantification. It was downloaded from imagej.net (https://imagej.net/software/fiji/) as a zip file bundled with Java.

3.1.3.1 Measurements of Brain Volume

For the Endpoint cohort, I measured cortical, hippocampal, hippocampal subregions and thalamic volume (Gail Canter et al., 2019) from a stereological series (1:10, see above). The images were scaled appropriately within Image J (W. Rasband, USA, version 2.3./1.53q). Regions of interest were identified based upon Allen brain atlas (https://mouse.brain-map.org/static/atlas) and outlined via Image J Software ROIs. The program calculated the outlined area. Volumes were then calculated using the Cavalieri method. All measurements were conducted by an observer blinded to the mouse genotype.

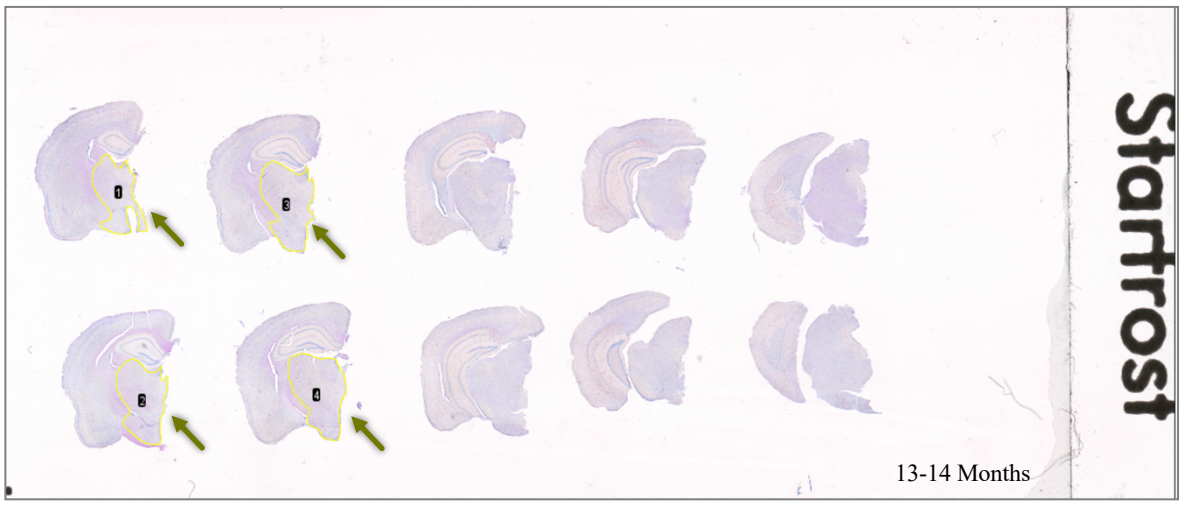

Figure 11. Volume analysis in serial coronal sections from the Endpoint study where photomicrographs were obtained using the Odyssey M Imaging System (LI-COR). The arrow shows the thalamus region segmented based on the brain atlas anatomy using Image J Software (W. Rasband, USA, version 2.3./1.53q). Thalamic volume was measured at the level of the hippocampus, from approximately -0.9mm AP to approximately -2.7mm AP, as more caudal levels are not possible to differentiate from midbrain without specific staining.

3.1.3.2 Imaging and Quantification of Congo Red Staining

Segmentation of positively stained pixels is easy when using Congo red-stained sections owing to the low background and high contrast of the stain. Images were opened in Image J Software (W. Rasband, USA, version 2.3./1.53q), scaled, then converted to RGB and then colour deconvolved using the Giemsa algorithm, which deconvolves the congo red and cresyl violet counter stain (see Fig 11). The Giemsa algorithm was chosen following extensive trialling to ensure appropriate deconvolution. Using the cresyl violet "blue" channel, the region of interest was outlined. This ROI was then placed upon the congo red channel (see "pink" channel C below). Following thresholding (0-150), plaques were distinguished and quantified using the Analyse Particles menu option. The analysis was applied to each image using a macro. The percent area occupied by total Congo red was determined for each image and recorded. See Figure 11 for the flow through of analysis.

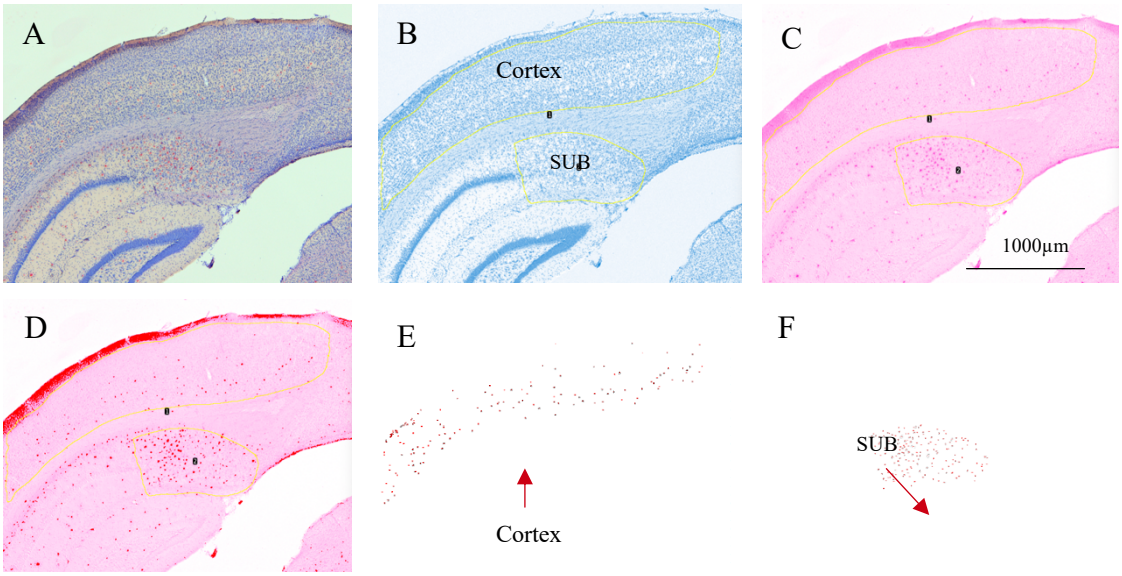

Figure 12. Representation of the image analysis protocol for the Congo Red quantification in the preclinical trial using Image J (W. Rasband, USA, version 2.3./1.53q). (A) shows the hippocampal area and cortex stained with Congo red and cresyl violet. The images were converted into RGB and then colours were deconvolved. (B) The "blue" channel preserved cresyl violet staining and was used to make an ROI of the region desired. (C) The "Pink" colour preserved the congo red staining and was used to analyse the plaques. (D) Representative thresholding for the plaques. (E) Example of plaques in cortex overlying sub, (F) and in Sub.

3.1.3.3 Imaging and Quantification of Thioflavin Staining

All images were captured with a fluorescence Stereo Zoom Microscope (ZEISS Axio Zoom.V16, Carl Zeiss Microscopy GmbH) and ZEISS ZEN Software Bundles (Carl Zeiss Microscopy GmbH). For analysing the amyloid, we utilized the Macro code in FIJI Image J (W. Rasband, USA, version 2.3./1.53q). All ROIs were defined by outlining with the polygon function located on the toolbar based on the Allen Mouse Brain Atlas markers. All images were converted into 8-bit grayscale and then auto-thresholded using the 'max entropy' filter. The filter was chosen following extensive trialling. In the final step of the ImageJ protocol, the "Analyze Particle" command under the Analyze tab was run to identify individual particles (plaques) within the ROI. The analysis was applied to each image using a macro. See Figure 12 for the flow of the analysis.

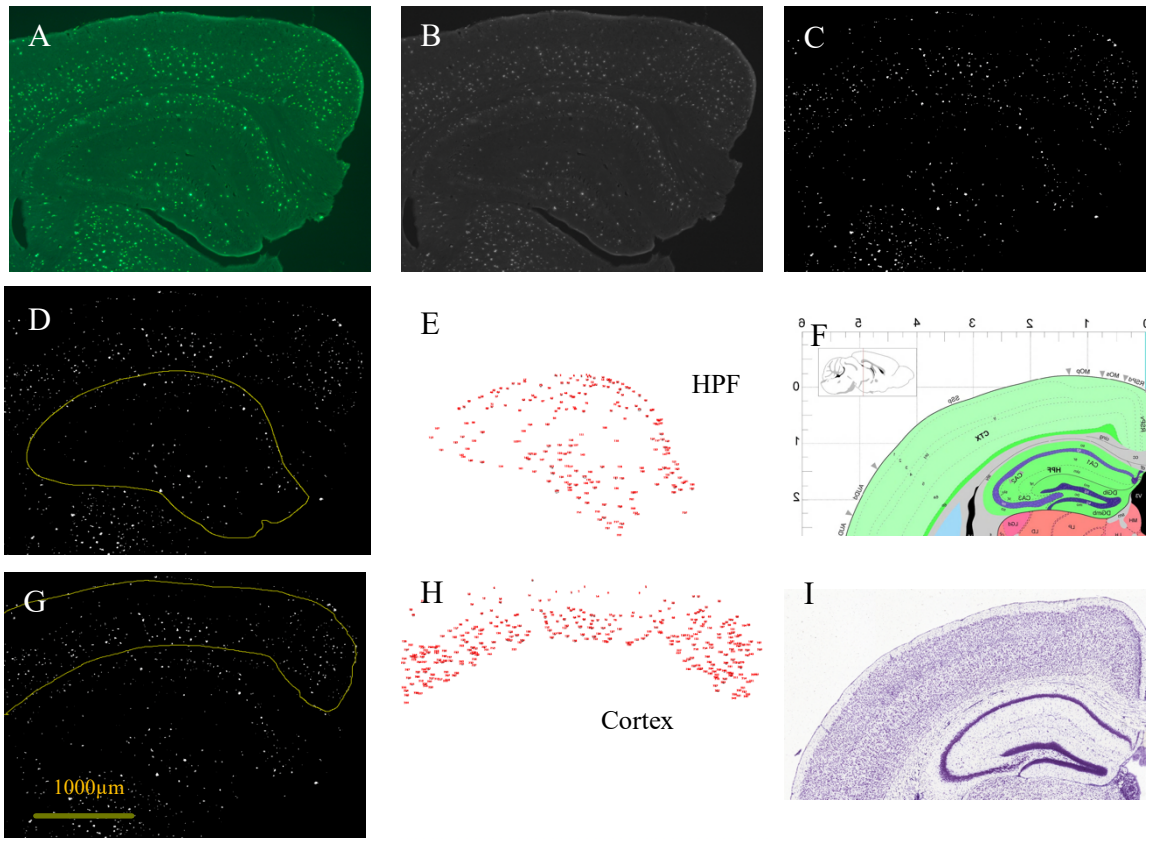

Figure 13. Representative image analysis protocol for the Thioflavin S quantification in the Endpoint cohort using Image J (W. Rasband, USA, version 2.3./1.53q). Scalebar x40. (A) shows the hippocampus area and cortex, stained with Thioflavin S (Bregma -1.855) (B) Images were converted to 8-bit grayscale, (C) and then auto-thresholded using the 'MaxEntropy' filter. (D) Example hippocampal and (G) overlying cortical ROI. (E,H) The "analyse particle" function is performed within the ROI, (F,I) Examples of the areas, images taken from the online Allen Mouse Brain atlas database shown for demonstration.

3.1.3.4 Imaging and Quantification of Astrocytes

All images were captured using confocal microscopy (Zeiss LSM780, Zen software 2010) and analysed with FIJI Image J software (W. Rasband, USA, version 2.3./1.53q). Most images were captured as a single image; however, due to some folding, two images were captured as a z-stack, which were made into maximum intensity projections. All images were separated into their channels (Red: GFAP; Blue: Hoechst) and converted to tifs. Tif files were then thresholded using the default auto-threshold tool and the percent area containing thresholded pixels was used for analysis. The analysis was applied to each image using a macro. For frontal somatosensory cortex, the entire cortex was analysed. For subiculum and overlying cortex, the region of interest was outlined based upon Hoechst images. These ROIs were then placed upon GFAP images for quantification of percent area containing GFAP signal above background. See Figure 13 for flow of analysis.

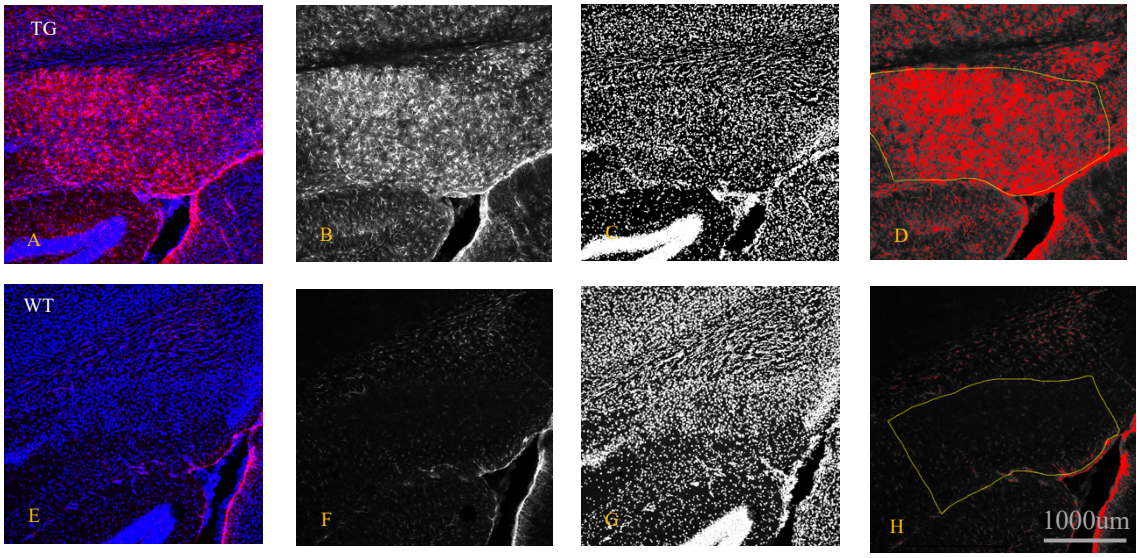

Figure 14. Representative flow of analysis of GFAP staining for the Preclinical trial using Image J (W. Rasband, USA, version 2.3./1.53q). Scalebar x10. (A,E) shows image (GFAP + Hoechst double immunofluorescence) captured with confocal microscopy (Zeiss LSM780) for a transgenic mouse (A) and a wildtype mouse (E). (B,F) GFAP staining (single channel, shown in black and white). The TG mouse clearly shows more astrocytes compared with the WT mouse. (C,G) Demonstrates Hoechst staining (reveals nuclei of all cells), which enables anatomy to be discerned. ROIs were drawn based upon Hoechst images. (D,H) Representative thresholded imaged with ROIs demonstrating the areas analysed.

3.1.4 Statistics

Depending upon the number of groups in the comparison, t-tests or 1-way ANOVAs were used to determine statistical differences. Post-hoc tests (Tukey's) were used to determine the source of variation, if 1-way ANOVAs were statistically significant. The critical value was set to $p < 0.05$. Data visualization and analysis was conducted using GraphPad Prism (GraphPad Software, CA, USA, V9.3.1.) software.

3.2 RESULTS

3.2.1 Endpoint Pathology in 13–14-month-old 5XFAD mice

Female 5XFAD mice showed reduced body weight in comparison to their female WT littermates which is consistent with earlier findings (Oblak et al., 2021). Notably, 5XFAD mice also demonstrated a decrease in brain weight, on a par with findings from female AD patient brains (Filon et al., 2016).

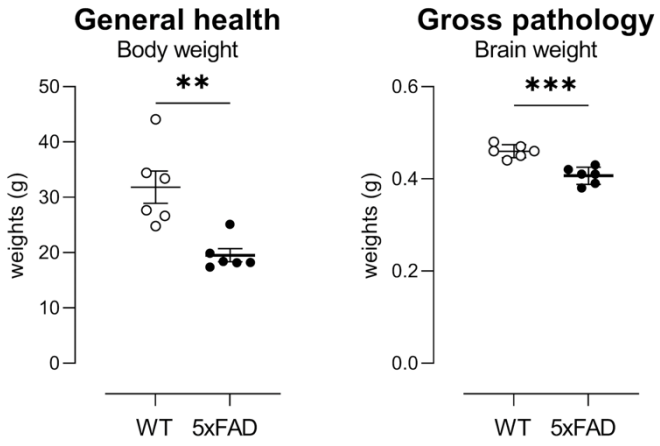

Figure 15. Body and brain weights expressed as grams, at 13-14 months of age. There were significant differences between WT and 5XFAD. Open data points are from WT animals and filled data points are from 5XFAD animals. Each point represents data from one animal. Horizontal bars show the mean ± SD. Data were compared using unpaired T-tests. **p<0.01, ***p<0.001

Although widely studied, we then examined regional atrophy in these old mice, to provide context for our preclinical trial and also to uncover novel regional atrophy to understand the major loss of parenchyma shown by brain weight analysis in Figure 14.

Manual segmentation was done after imaging based on the landmarks of Allen Mouse Brain Atlas on photomicrographs stained with congo red and cresyl violet. Our results showed there is no significant differences in volume of cortex overlying hippocampus or in total hippocampus between old 5xFAD TG mice and their wild type littermates. No difference in sub-regional volumes, in SUB, CA1, CA2-3 or DG were detected either (Figure 16).

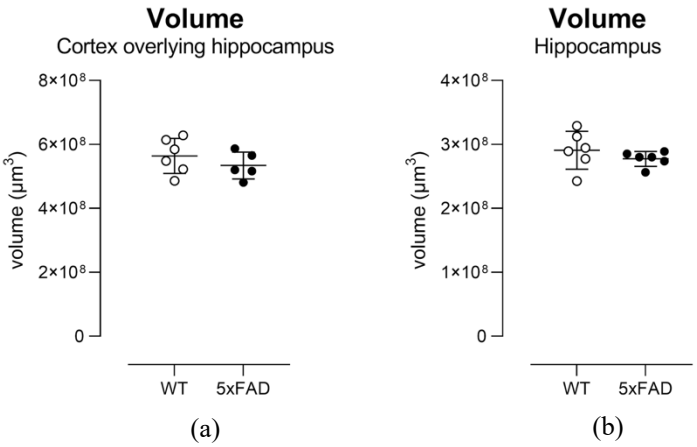

Figure 16. Volume analysis at 13-14-month-of-age 5XFAD mice and their WT littermates (all female). (a), Cortex overlying hippocampus (b), Hippocampus. There were no significant differences between WT and 5XFAD. ($p < 0.05$, statistically nonsignificant difference.) Horizontal bars show the mean ± SD.

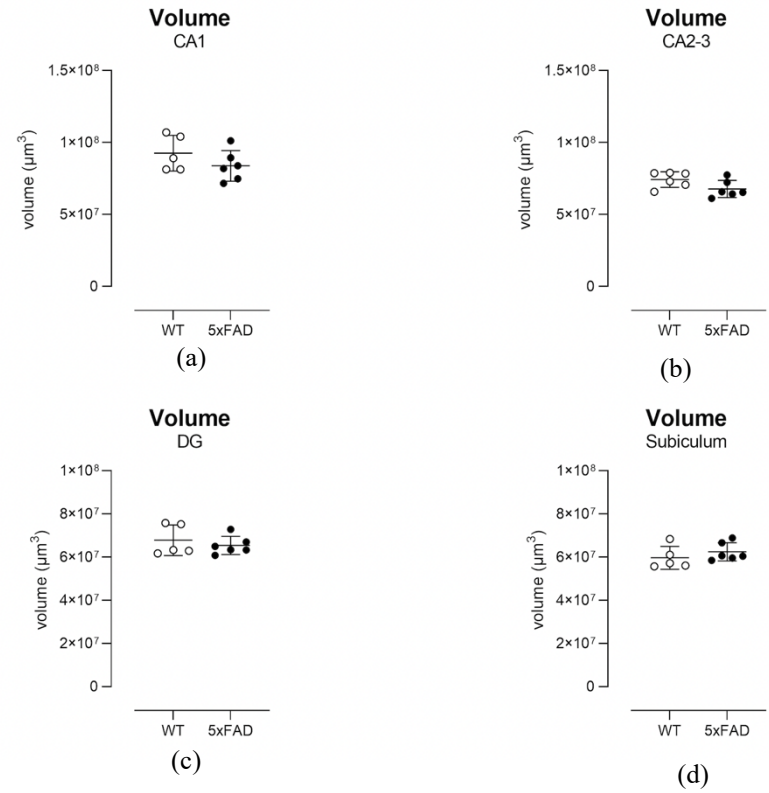

Figure 17. Volume analysis of hippocampal subfields. (a) CA1, (b) CA2-3, (c) DG and (d) Subiculum. There were no statistically significant differences between wild type littermate and transgenic mice (all female littermates). Horizontal bars show the mean ± SD.

Interestingly, recent data from patients and indeed, 5xFAD mice, show that the earliest pathology is not limited to the temporal cortex but rather widespread throughout the Papez network, and includes the thalamus. Indeed, patient carriers of mutations in presenilin 1 show consistent loss of volume of thalamus with hippocampal atrophy being less consistent (Aggleton et al., 2016). We therefore examined thalamus and indeed found a slight reduction in volume in our Endpoint TG mice. Our findings demonstrate that thalamus is more affected than hippocampus.

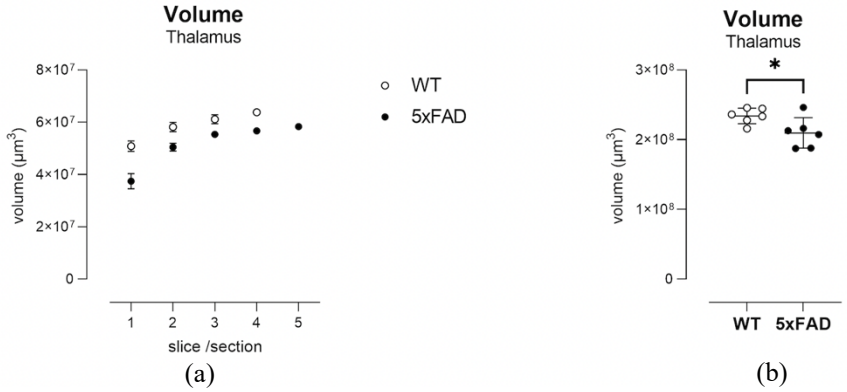

Figure 18. Thalamic volume in 13-14 months of age female 5XFAD mice and their female WT littermates. (Left) Stereological analysis of thalamus in WT versus TG showing that volume is much reduced at each successive cryosection in the stereological series. Note: the stereological series do not contain sections that are identical at every section by design; this is an inherent, important characteristic for stereological series (Lerner et al., 2012) and it ensures that the series are random for each mouse. Hence the 5th 5xFAD slice/section, from one mouse, whose stereological series happened to begin at a very rostral point. (Right) total thalamus volume in WT versus TG, unpaired t-test $p<0.05$. Data show mean ± sem (left) and mean ± SD (right).

3.2.2 Patterns of amyloid deposition in the 5XFAD

To provide further context for our preclinical trial, we then went on to determine sizes of plaques and plaque densities in our Endpoint cohort. Aβ deposition first appears in the cortex , hippocampus, and thalamus of 5xFAD mice at 1.5 months of age. We performed thioflavin s as well as congo red staining. we assess the Aβ in the cortex overlying hippocampus, hippocampus, and the subiculum in Endpoint cohort. The quantification revealed that the Aβ deposition was more significant in subiculum in compared to hippocampus and cortex, as expected. Despite the lack of atrophy in subiculum, plaque density was much greater in this nucleus compared with hippocampus or cortex.

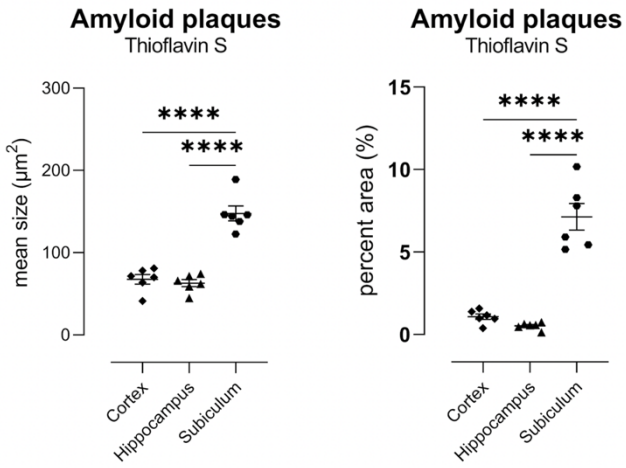

Figure 19. Plaque quantification in Cortex, Hippocampus and Subiculum using Thioflavin S to detect Aβ. Female TG mice were used for analysis only as WT mice do not show plaques. Left: 1-way ANOVA F (2, 15) = 50,66, p<0.0001 followed by Tukey's post hoc tests, ****p < 0.0001. Right: 1-way ANOVA F (2, 15) = 59,46, p<0.001 followed by Tukey's post hoc tests, ****p < 0.0001. Data show mean ± sem. Data points are of individual mice.

3.2.3 Preclinical trial of nanoformulated BDMC in 5xFAD mice.

3.2.3.1 Effect on plaques determined using ThioS and congo red

For the preclinical trial, Thioflavin S and Congo red staining were performed to examine potential treatment effects of nanoformulation BDMC on plaques. Our group sizes were WT saline:16, TG saline:12, TG BDMC:12. All mice were females. Mice were pseudorandomized to their treatment groups to ensure appropriate littermate controls. These group sizes are adequately powered to detect treatment effects (congo red, GFAP; N=4 required to detect a reduction of 50% with 80% power and alpha set to 0.05).

There was no significant difference in percent area or plaque size between the treated and untreated cohort in preclinical trial as determined by ThioS (Fig 19). Indeed, congo red staining showed increased plaque size in frontal cortex (Fig 20), and although a similar trend was observed with ThioS, it did not reach significance due to the variability in this outcome measure.

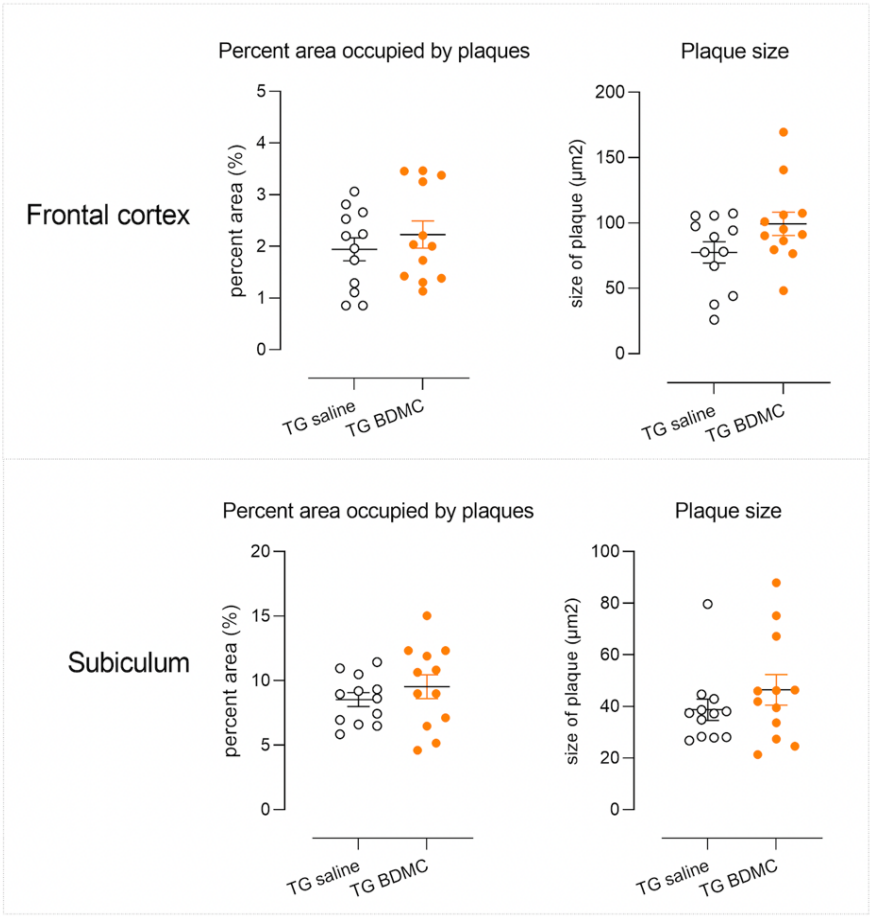

Figure 20. Plaque quantification in Frontal cortex and Subiculum using Thioflavin S to detect Aβ in the preclinical trial. There were no significant differences between treated and non-treated transgenic mice. Female TG mice from the trial were used for analysis only as WT mice do not show plaques. Data show mean ± sem. Data points are of individual mice.

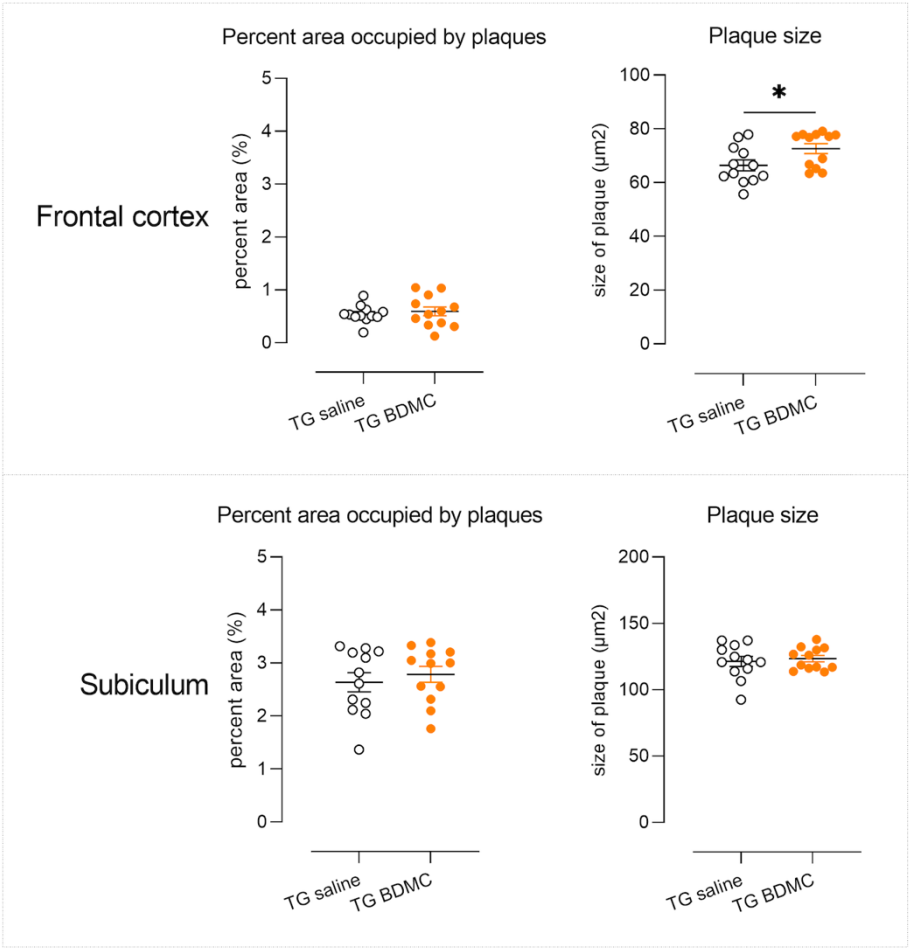

Figure 21. Plaque quantification in Frontal cortex and Subiculum using Congo red to detect Aβ in the preclinical trial. Congo red (for plaques) and cresyl violet (for anatomy) were used to stain the images. There were no significant changes between transgenic mice that were treated and those who were not. However, there was a small increase in plaque size in the frontal cortex. Data show mean ± sem. Data points are of individual mice. Data compared using unpaired t-tests, *p<0.05.

3.2.3.2 Effect on astrocytes determined using immunofluorescence

Neuroinflammation is characterized by the presence of activated astrocytes and microglia surrounding amyloid plaques in AD patient tissue. Neuroinflammation is well known and characterized in the 5XFAD mice.

Astrocytes were quantified in frontal somatosensory cortex, caudal cortex (visual cortex) overlying subiculum and in subiculum. As expected for mice of this age (8-9 months), I confirmed a very significant genotype effect, as TG groups showed much greater levels of astrocytosis than WT littermates (frontal cortex $F(2, 32) = 10{,}21$, $p<0.01$; caudal cortex $F(2, 34) = 9{,}448$, $p<0.001$; subiculum, $F(2, 34) = 8{,}100$, $p<0.002$). However, there was no difference between TG groups, indicating that nanoformulated BDMC did not ameliorate the extensive astrocytosis in this model.

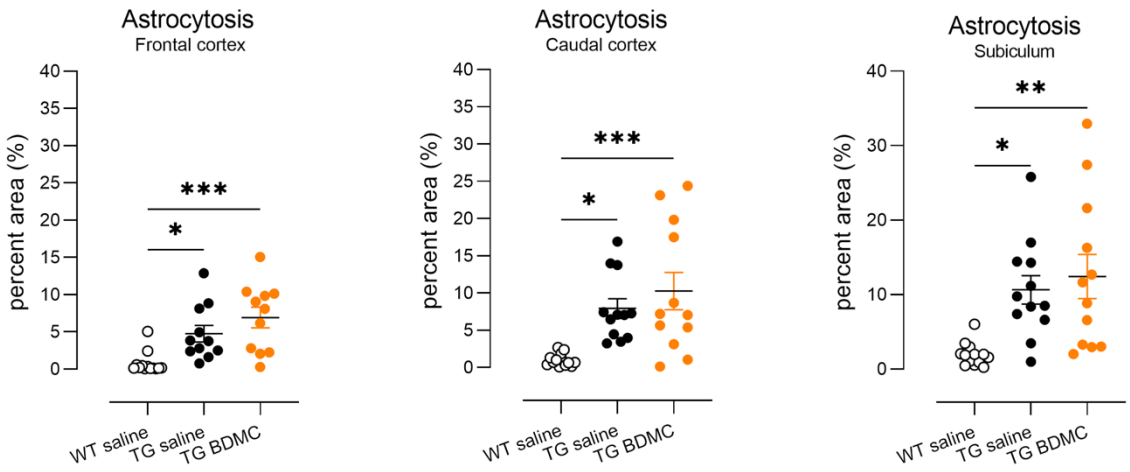

Figure 22. Astrocytosis in frontal somatosensory cortex, caudal (visual) cortex and in subiculum using immunofluorescence to detect GFAP, a marker of astrocytes in the preclinical trial. The percentage area of astrocytes, as detected by signal above background was calculated. No significant difference in percent area was observed between TG control and TG treated mice. A large significant difference was detected between WT littermates and each TG group. * $p<0.05$, ** $p<0.01$, *** $p< 0.001$. Data show mean ± sem. Data points are of individual mice. Data were compared using 1-way ANOVAs, followed by Tukey's post-hoc tests. See text for F statistics.

3.3 DISCUSSION

Accumulation of beta-amyloid (Aβ) contributes to neurodegeneration and memory loss in Alzheimer's disease; however, regional differences in Aβ occur and there are unexpectedly high densities in small subcortical nuclei that develop in the 5XFAD animals over time (Gail Canter et al., 2019).

Despite its long use, there is much still to be learned of the 5xFAD mice. For example, although reviews (Webster et al., 2014) suggest extensive cognitive impairment, recent data, and our own, show that cognitive impairment is very mild in these mice (Oblak et al., 2021), and that motor impairment may be a more robust outcome measure for behaviour (Forner et al., 2021). Moreover, although tradition states that these mice do not accumulate tau, some authors have found evidence of tau accumulation with age (Mattsson-Carlgren et al., 2020). Some authors have reported neuronal loss within Layer V pyramidal neurons of the cortex (Eimer & Vassar, 2013); however, hippocampal atrophy is not consistently observed (Jullienne et al., 2022). Thus, we asked whether other areas should be examined.

Recent data suggests the involvement of the thalamus at early stages of neuropathology in familial AD, particularly in thalamus, an area that also shows extensive amyloid deposition (Cash et al., 2013; Harper et al., 2017; Pardilla-Delgado et al., 2020). In our Endpoint cohort, we therefore examined several regions, including traditional regions of interest such as the cortex and hippocampus and hippocampal subregions and also the thalamus. We note that at Endpoint, the TG mice weighed substantially less than their WT littermates (almost 40% less) and their brain weights were also reduced by 12%. Previous data from patients suggest 6-9% atrophy at autopsy in male and female patients, respectively (Filon et al., 2016). Thus, 5xFAD mice show profound atrophy but detailed analysis reveals that this does not translate to volume loss in traditional areas such as hippocampus or cortex, as has been shown previously and as we show here. Significantly, we now show atrophy of the thalamus in aged 5xFAD mice, similar to findings in familial AD. Moreover, our data support recent data from large-tissue volume processing in the 5XFAD mice that revealed early involvement of thalamus in 5xFAD amyloid deposition, possibly because it is a node within the Papez memory circuit (Gail Canter et al., 2019).

We then went on to examine the effect of a novel therapeutic, nanoformulated bisdemethoxycurcumin, in a preclinical trial in these mice. Importantly, a recent review of over 400 preclinical therapeutic trials in AD transgenic mice showed no sample size calculation. The authors suggested this may underlie the typically small sample sizes used

(N=7 in control groups, N=9 in mutant groups)(Egan & Macleod, 2014) in preclinical trials. As an example of how important this is, underpowered preclinical studies were identified as the single most important factor that contributed to failure of a therapeutic in human ALS patients (Scott et al., 2008). Here, we used large group sizes and previously calculated sample sizes ensured that we had power to detect treatment effects (congo red, GFAP; N=4 required to detect a reduction of 50% with 80% power and alpha set to 0.05). BDMC is a curcuminoid, that is naturally occurring the rhizomes of the *Curcuma longa* plant. We are unaware of previous in vivo efficacy trials of BDMC in a genetic mouse model of AD.

Mice were injected twice weekly (intraperitoneally), for 2 months, from 6-7 months of age until 8-9 months of age. Mice were carefully matched for age and for littermates to ensure groups were well balanced and of sufficient size as this is a continuing issue in AD preclinical trials. Our trial design adheres to ARRIVE guidelines (Percie du Sert et al., 2020).

Despite the fact that BDMC appears to bind amyloid strongly, we find no evidence of reduced plaque burden in the 5xFAD – if anything plaque size was increased, as revealed by congo red, with a similar but non-significant trend observed in ThioS staining. Although widely used in the clinic for analysis of amyloid, congo red and ThioS staining may not be completely specific for amyloid (Yakupova et al., 2019), and future work shall include confirmation of results with MOAB2, an antibody that is highly specific for Aβ (Youmans et al., 2012). Moreover, at high concentrations, curcumin, another curcuminoid, can increase huntingtin amyloid plaque size in vitro (Hickey et al., 2012); however, whether BDMC mimics these findings and reaches these high concentrations in our mice is unclear. In future experiments, we shall examine green fluorescence (BDMC is fluorescent)(den Haan et al., 2018) in unlabelled sections as this may provide relative data on BDMC content in our regions of interest. Moreover, this would provide information on whether ThioS data, which were more variable than congo red data, particularly in the treated group, were influenced by fluorescence from BDMC. In our previous preclinical trial with nano-formulated curcumin, we found no such effect; thus, the nanoformulation of H-Ferritin itself is unlikely to be a contributing factor. Finally, we note that BDMC binds neurofibrillary tangles (den Haan et al., 2018). Although tangles are not a well-known outcome measure in 5xFAD mice, others have reported that tau ThioS may bind tau thereby obscuring specific effects on amyloid (Shin et al., 2021).

Astrocytes have been shown to influence synaptic activity and glutamate balance, blood-brain barrier (BBB) development and neurovascular coupling, and the inflammatory response. Other proteins related to neurodegeneration, such as tau and a-synuclein, can accumulate in astrocytes. When co-cultured with neonatal neurons, astrocytes extracted from

aged 5xFAD mice provide much less neurotrophic support than astrocytes derived from wild-type mice (Perez-Nievas & Serrano-Pozo, 2018). We also evaluated astrocytes with anti-GFAP immunofluorescence in the preclinical trial. BDMC did not reduce inflammation in the frontal somatosensory cortex, visual cortex or subiculum.

It is possible that higher doses of BDMC are required, as curcumin has been proven to be more powerful as an antioxidant than demethoxycurcumin, which in turn is more effective than BDMC (Somparn et al., 2007). Nevertheless, given our findings, BDMC does not appear to be beneficial in AD.

SUMMARY

This research aimed to examine end-stage pathology in 5xFAD mice at 13-14 months of age. Based on the brain volume analysis and amyloid analysis, our data confirm previous data on hippocampal and cortical volumes. However, in keeping with recent findings from patients with familial AD where reduced thalamic volume is more consistently observed than reduced hippocampal volume, we found reduced thalamic volume in our stereological analysis of 5xFAD mice, which carry five separate mutations that individually lead to AD in humans. Future work could include consideration of the thalamus in our preclinical trials. Indeed, another aim was analysing the effect of a novel therapeutic, nano-formulated Bisdemethoxycurcumin, on neuropathology of 5xFAD mice. Mice were treated for 2 months, and we determined that there were no significant changes between treated and control TG mice in inflammation (astrocytosis) and no overall effect on amyloidosis. Indeed, treated TG mice tended to show increased plaque size, particularly in frontal somatosensory cortex. Future work shall focus on the analysis of amyloid using more specific anti-amyloid antibodies, and on microgliosis, an additional critical inflammatory change observed in these mice.

REFERENCES

Aggleton, J. P., Pralus, A., Nelson, A. J. D., & Hornberger, M. (2016). Thalamic pathology and memory loss in early Alzheimer's disease: moving the focus from the medial temporal lobe to Papez circuit. *Brain*, *139*(7), 1877–1890. https://doi.org/10.1093/brain/aww083

Awada, A. A. (2015). Early and late-onset Alzheimer's disease: What are the differences? *Journal of Neurosciences in Rural Practice*, *6*(03), 455–456. https://doi.org/10.4103/0976-3147.154581

Bishara, D., Sauer, J., & Taylor, D. (2015). The pharmacological management of Alzheimer's disease. *Progress in Neurology and Psychiatry*, *19*(4), 9–16. https://doi.org/10.1002/pnp.387

Cash, D. M., Ridgway, G. R., Liang, Y., Ryan, N. S., Kinnunen, K. M., Yeatman, T., Malone, I. B., Benzinger, T. L. S., Jack, C. R., Thompson, P. M., Ghetti, B. F., Saykin, A. J., Masters, C. L., Ringman, J. M., Salloway, S. P., Schofield, P. R., Sperling, R. A., Cairns, N. J., Marcus, D. S., … Fox, N. C. (2013). The pattern of atrophy in familial Alzheimer disease: Volumetric MRI results from the DIAN study. *Neurology*, *81*(16), 1425–1433. https://doi.org/10.1212/WNL.0b013e3182a841c6

Congdon, E. E., & Sigurdsson, E. M. (2018). Tau-targeting therapies for Alzheimer disease. *Nature Reviews Neurology*, *14*(7), 399–415. https://doi.org/10.1038/s41582-018-0013-z

den Haan, J., Morrema, T. H. J., Rozemuller, A. J., Bouwman, F. H., & Hoozemans, J. J. M. (2018). Different curcumin forms selectively bind fibrillar amyloid beta in post mortem Alzheimer's disease brains: Implications for in-vivo diagnostics. *Acta Neuropathologica Communications*, *6*(1), 75. https://doi.org/10.1186/s40478-018-0577-2

di Meo, F., Margarucci, S., Galderisi, U., Crispi, S., & Peluso, G. (2019). Curcumin, gut microbiota, and neuroprotection. In *Nutrients* (Vol. 11, Issue 10). https://doi.org/10.3390/nu11102426

Egan, K., & Macleod, M. (2014). Two decades testing interventions in transgenic mouse models of Alzheimer's disease: designing and interpreting studies for clinical trial success. *Clinical Investigation*, *4*(8), 693–704. https://doi.org/10.4155/cli.14.55

Ege, D. (2021). Action mechanisms of curcumin in alzheimer's disease and its brain targeted delivery. In *Materials* (Vol. 14, Issue 12). https://doi.org/10.3390/ma14123332

Eimer, W. A., & Vassar, R. (2013). Neuron loss in the 5XFAD mouse model of Alzheimer's disease correlates with intraneuronal Aβ42 accumulation and Caspase-3 activation. *Molecular Neurodegeneration*, *8*(1), 2. https://doi.org/10.1186/1750-1326-8-2

Elder, G. A., Gama Sosa, M. A., & de Gasperi, R. (2010). Transgenic Mouse Models of Alzheimer's Disease. *Mount Sinai Journal of Medicine: A Journal of Translational and Personalized Medicine*, *77*(1), 69–81. https://doi.org/10.1002/msj.20159

Feng, B. Y., & Shoichet, B. K. (2006). A detergent-based assay for the detection of promiscuous inhibitors. *Nature Protocols*, *1*(2), 550–553. https://doi.org/10.1038/nprot.2006.77

Filon, J. R., Intorcia, A. J., Sue, L. I., Vazquez Arreola, E., Wilson, J., Davis, K. J., Sabbagh, M. N., Belden, C. M., Caselli, R. J., Adler, C. H., Woodruff, B. K., Rapscak, S. Z., Ahern, G. L., Burke, A. D., Jacobson, S., Shill, H. A., Driver-Dunckley, E., Chen, K., Reiman, E. M., … Serrano, G. E. (2016). Gender Differences in Alzheimer Disease: Brain Atrophy, Histopathology Burden, and Cognition. *Journal of Neuropathology & Experimental Neurology*, *75*(8), 748–754. https://doi.org/10.1093/jnen/nlw047

Forner, S., Kawauchi, S., Balderrama-Gutierrez, G., Kramár, E. A., Matheos, D. P., Phan, J., Javonillo, D. I., Tran, K. M., Hingco, E., da Cunha, C., Rezaie, N., Alcantara, J. A., Baglietto-Vargas, D., Jansen, C., Neumann, J., Wood, M. A., MacGregor, G. R., Mortazavi, A., Tenner, A. J., … Green, K. N. (2021). Systematic phenotyping and

characterization of the 5xFAD mouse model of Alzheimer's disease. *Scientific Data*, *8*(1), 270. https://doi.org/10.1038/s41597-021-01054-y

Frisoni, G. B., Altomare, D., Thal, D. R., Ribaldi, F., van der Kant, R., Ossenkoppele, R., Blennow, K., Cummings, J., van Duijn, C., Nilsson, P. M., Dietrich, P.-Y., Scheltens, P., & Dubois, B. (2022). The probabilistic model of Alzheimer disease: the amyloid hypothesis revised. *Nature Reviews Neuroscience*, *23*(1), 53–66. https://doi.org/10.1038/s41583-021-00533-w

Gagliardi, S., Morasso, C., Stivaktakis, P., Pandini, C., Tinelli, V., Tsatsakis, A., Prosperi, D., Hickey, M., Corsi, F., & Cereda, C. (2020). Curcumin Formulations and Trials: What's New in Neurological Diseases. *Molecules*, *25*(22), 5389. https://doi.org/10.3390/molecules25225389

Gail Canter, R., Huang, W.-C., Choi, H., Wang, J., Ashley Watson, L., Yao, C. G., Abdurrob, F., Bousleiman, S. M., Young, J. Z., Bennett, D. A., Delalle, I., Chung, K., & Tsai, L.-H. (2019). 3D mapping reveals network-specific amyloid progression and subcortical susceptibility in mice. *Communications Biology*, *2*(1), 360. https://doi.org/10.1038/s42003-019-0599-8

Hampel, H., Mesulam, M.-M., Cuello, A. C., Farlow, M. R., Giacobini, E., Grossberg, G. T., Khachaturian, A. S., Vergallo, A., Cavedo, E., Snyder, P. J., & Khachaturian, Z. S. (2018). The cholinergic system in the pathophysiology and treatment of Alzheimer's disease. *Brain*, *141*(7), 1917–1933. https://doi.org/10.1093/brain/awy132

Harper, L., Bouwman, F., Burton, E. J., Barkhof, F., Scheltens, P., O'Brien, J. T., Fox, N. C., Ridgway, G. R., & Schott, J. M. (2017). Patterns of atrophy in pathologically confirmed dementias: a voxelwise analysis. *Journal of Neurology, Neurosurgery & Psychiatry*, *88*(11), 908–916. https://doi.org/10.1136/jnnp-2016-314978

Heneka, M. T., Carson, M. J., Khoury, J. el, Landreth, G. E., Brosseron, F., Feinstein, D. L., Jacobs, A. H., Wyss-Coray, T., Vitorica, J., Ransohoff, R. M., Herrup, K., Frautschy, S. A., Finsen, B., Brown, G. C., Verkhratsky, A., Yamanaka, K., Koistinaho, J., Latz, E., Halle, A., … Kummer, M. P. (2015). Neuroinflammation in Alzheimer's disease. *The Lancet Neurology*, *14*(4), 388–405. https://doi.org/10.1016/S1474-4422(15)70016-5

Hickey, M. A., Zhu, C., Medvedeva, V., Lerner, R. P., Patassini, S., Franich, N. R., Maiti, P., Frautschy, S. A., Zeitlin, S., Levine, M. S., & Chesselet, M.-F. (2012). Improvement of neuropathology and transcriptional deficits in CAG 140 knock-in mice supports a beneficial effect of dietary curcumin in Huntington's disease. *Molecular Neurodegeneration*, *7*(1), 12. https://doi.org/10.1186/1750-1326-7-12

Jansen, W. J., Ossenkoppele, R., Knol, D. L., Tijms, B. M., Scheltens, P., Verhey, F. R. J., Visser, P. J., Aalten, P., Aarsland, D., Alcolea, D., Alexander, M., Almdahl, I. S., Arnold, S. E., Baldeiras, I., Barthel, H., van Berckel, B. N. M., Bibeau, K., Blennow, K., Brooks, D. J., … Zetterberg, H. (2015). Prevalence of Cerebral Amyloid Pathology in Persons Without Dementia. *JAMA*, *313*(19), 1924. https://doi.org/10.1001/jama.2015.4668

Jha, A., & Mukhopadhaya, K. (2021). *Alzheimer's Disease*.

Jouanne, M., Rault, S., & Voisin-Chiret, A.-S. (2017). Tau protein aggregation in Alzheimer's disease: An attractive target for the development of novel therapeutic agents. *European Journal of Medicinal Chemistry*, *139*, 153–167. https://doi.org/10.1016/j.ejmech.2017.07.070

Jullienne, A., Trinh, M. v., & Obenaus, A. (2022). Neuroimaging of Mouse Models of Alzheimer's Disease. *Biomedicines*, *10*(2), 305. https://doi.org/10.3390/biomedicines10020305

Kametani, F., & Hasegawa, M. (2018). Reconsideration of Amyloid Hypothesis and Tau Hypothesis in Alzheimer's Disease. *Frontiers in Neuroscience*, *12*. https://doi.org/10.3389/fnins.2018.00025

Kukull, W. A., & Bowen, J. D. (2002). Dementia epidemiology. *Medical Clinics of North America*, *86*(3), 573–590. https://doi.org/10.1016/S0025-7125(02)00010-X

Lane, C. A., Hardy, J., & Schott, J. M. (2018). Alzheimer's disease. *European Journal of Neurology*, *25*(1), 59–70. https://doi.org/10.1111/ene.13439

Leng, F., & Edison, P. (2021). Neuroinflammation and microglial activation in Alzheimer disease: where do we go from here? *Nature Reviews Neurology*, *17*(3), 157–172. https://doi.org/10.1038/s41582-020-00435-y

Lerner, R. P., Trejo Martinez, L. del C. G., Zhu, C., Chesselet, M.-F., & Hickey, M. A. (2012). Striatal atrophy and dendritic alterations in a knock-in mouse model of Huntington's disease. *Brain Research Bulletin*, *87*(6), 571–578. https://doi.org/10.1016/j.brainresbull.2012.01.012

lo Cascio, F., Marzullo, P., Kayed, R., & Palumbo Piccionello, A. (2021). Curcumin as Scaffold for Drug Discovery against Neurodegenerative Diseases. *Biomedicines*, *9*(2), 173. https://doi.org/10.3390/biomedicines9020173

Long, J. M., & Holtzman, D. M. (2019). Alzheimer Disease: An Update on Pathobiology and Treatment Strategies. *Cell*, *179*(2), 312–339. https://doi.org/10.1016/j.cell.2019.09.001

Maiti, P., Hall, T. C., Paladugu, L., Kolli, N., Learman, C., Rossignol, J., & Dunbar, G. L. (2016). A comparative study of dietary curcumin, nanocurcumin, and other classical amyloid-binding dyes for labeling and imaging of amyloid plaques in brain tissue of 5×-familial Alzheimer's disease mice. *Histochemistry and Cell Biology*, *146*(5), 609–625. https://doi.org/10.1007/s00418-016-1464-1

Mattsson-Carlgren, N., Andersson, E., Janelidze, S., Ossenkoppele, R., Insel, P., Strandberg, O., Zetterberg, H., Rosen, H. J., Rabinovici, G., Chai, X., Blennow, K., Dage, J. L., Stomrud, E., Smith, R., Palmqvist, S., & Hansson, O. (2020). Aβ deposition is associated with increases in soluble and phosphorylated tau that precede a positive Tau PET in Alzheimer's disease. *Science Advances*, *6*(16). https://doi.org/10.1126/sciadv.aaz2387

Myers, A., & McGonigle, P. (2019). Overview of Transgenic Mouse Models for Alzheimer's Disease. *Current Protocols in Neuroscience*, *89*(1). https://doi.org/10.1002/cpns.81

Oakley, H., Cole, S. L., Logan, S., Maus, E., Shao, P., Craft, J., Guillozet-Bongaarts, A., Ohno, M., Disterhoft, J., van Eldik, L., Berry, R., & Vassar, R. (2006). Intraneuronal beta-Amyloid Aggregates, Neurodegeneration, and Neuron Loss in Transgenic Mice with Five Familial Alzheimer's Disease Mutations: Potential Factors in Amyloid Plaque Formation. *Journal of Neuroscience*, *26*(40), 10129–10140. https://doi.org/10.1523/JNEUROSCI.1202-06.2006

Oblak, A. L., Lin, P. B., Kotredes, K. P., Pandey, R. S., Garceau, D., Williams, H. M., Uyar, A., O'Rourke, R., O'Rourke, S., Ingraham, C., Bednarczyk, D., Belanger, M., Cope, Z. A., Little, G. J., Williams, S.-P. G., Ash, C., Bleckert, A., Ragan, T., Logsdon, B. A., … Lamb, B. T. (2021). Comprehensive Evaluation of the 5XFAD Mouse Model for Preclinical Testing Applications: A MODEL-AD Study. *Frontiers in Aging Neuroscience*, *13*. https://doi.org/10.3389/fnagi.2021.713726

Pandolfi, L., Bellini, M., Vanna, R., Morasso, C., Zago, A., Carcano, S., Avvakumova, S., Bertolini, J. A., Rizzuto, M. A., Colombo, M., & Prosperi, D. (2017). H-Ferritin Enriches the Curcumin Uptake and Improves the Therapeutic Efficacy in Triple Negative Breast Cancer Cells. *Biomacromolecules*, *18*(10), 3318–3330. https://doi.org/10.1021/acs.biomac.7b00974

Pardilla-Delgado, E., Torrico-Teave, H., Ramirez-Gomez, L. A., Baena, A., Bocanegra, Y., Vila-Castelar, C., Fox-Fuller, J. T., Guzman-Velez, E., Martínez, J., Sanchez, J. S., Lopera, F., & Quiroz, Y. T. (2020). Reduced thalamic volume is associated with early

brain pathology in preclinical autosomal dominant Alzheimer's disease. *Alzheimer's & Dementia*, *16*(S4). https://doi.org/10.1002/alz.046347

Percie du Sert, N., Hurst, V., Ahluwalia, A., Alam, S., Avey, M. T., Baker, M., Browne, W. J., Clark, A., Cuthill, I. C., Dirnagl, U., Emerson, M., Garner, P., Holgate, S. T., Howells, D. W., Karp, N. A., Lazic, S. E., Lidster, K., MacCallum, C. J., Macleod, M., … Würbel, H. (2020). The ARRIVE guidelines 2.0: Updated guidelines for reporting animal research. *PLOS Biology*, *18*(7), e3000410. https://doi.org/10.1371/journal.pbio.3000410

Polanco, J. C., Li, C., Bodea, L.-G., Martinez-Marmol, R., Meunier, F. A., & Götz, J. (2018). Amyloid-β and tau complexity — towards improved biomarkers and targeted therapies. *Nature Reviews Neurology*, *14*(1), 22–39. https://doi.org/10.1038/nrneurol.2017.162

Radbakhsh, S., Barreto, G. E., Bland, A. R., & Sahebkar, A. (2021). Curcumin: A small molecule with big functionality against amyloid aggregation in neurodegenerative diseases and type 2 diabetes. *BioFactors*, *47*(4), 570–586. https://doi.org/10.1002/biof.1735

Rossano, S. M., & Kreisl, W. C. (2021). Untangling the relationship between microglia and tau in Alzheimer's disease. *Trends in Neurosciences*, *44*(12), 927–929. https://doi.org/10.1016/j.tins.2021.10.002

Scheltens, P., de Strooper, B., Kivipelto, M., Holstege, H., Chételat, G., Teunissen, C. E., Cummings, J., & van der Flier, W. M. (2021). Alzheimer's disease. *The Lancet*, *397*(10284), 1577–1590. https://doi.org/10.1016/S0140-6736(20)32205-4

Scott, S., Kranz, J. E., Cole, J., Lincecum, J. M., Thompson, K., Kelly, N., Bostrom, A., Theodoss, J., Al-Nakhala, B. M., Vieira, F. G., Ramasubbu, J., & Heywood, J. A. (2008). Design, power, and interpretation of studies in the standard murine model of ALS. *Amyotrophic Lateral Sclerosis*, *9*(1), 4–15. https://doi.org/10.1080/17482960701856300

Shahryari, V., Nip, H., Saini, S., Dar, A. A., Yamamura, S., Mitsui, Y., Colden, M., Bucay, N., Tabatabai, L. Z., Greene, K., Deng, G., Tanaka, Y., Dahiya, R., & Majid, S. (2016). Pre-clinical Orthotopic Murine Model of Human Prostate Cancer. *Journal of Visualized Experiments*, *114*. https://doi.org/10.3791/54125

Sharma, R. A., Gescher, A. J., & Steward, W. P. (2005). Curcumin: The story so far. *European Journal of Cancer*, *41*(13), 1955–1968. https://doi.org/10.1016/j.ejca.2005.05.009

Shin, J., Park, S., Lee, H., & Kim, Y. (2021). Thioflavin-positive tau aggregates complicating quantification of amyloid plaques in the brain of 5XFAD transgenic mouse model. *Scientific Reports*, *11*(1), 1617. https://doi.org/10.1038/s41598-021-81304-6

Somparn, P., Phisalaphong, C., Nakornchai, S., Unchern, S., & Morales, N. P. (2007). Comparative Antioxidant Activities of Curcumin and Its Demethoxy and Hydrogenated Derivatives. *Biological and Pharmaceutical Bulletin*, *30*(1), 74–78. https://doi.org/10.1248/bpb.30.74

Tai, L. M., Maldonado Weng, J., LaDu, M. J., & Brady, S. T. (2021). *Relevance of transgenic mouse models for Alzheimer's disease* (pp. 1–48). https://doi.org/10.1016/bs.pmbts.2020.07.007

Tombaugh, T. N., McDowell, I., Kristjansson, B., & Hubley, A. M. (1996). Mini-Mental State Examination (MMSE) and the Modified MMSE (3MS): A psychometric comparison and normative data. *Psychological Assessment*, *8*(1), 48–59. https://doi.org/10.1037/1040-3590.8.1.48

van der Kant, R., Goldstein, L. S. B., & Ossenkoppele, R. (2020). Amyloid-β-independent regulators of tau pathology in Alzheimer disease. *Nature Reviews Neuroscience*, *21*(1), 21–35. https://doi.org/10.1038/s41583-019-0240-3

Veldman, E. R., Jia, Z., Halldin, C., & Svedberg, M. M. (2016a). Amyloid binding properties of curcumin analogues in Alzheimer's disease postmortem brain tissue. *Neuroscience Letters*, *630*, 183–188. https://doi.org/10.1016/j.neulet.2016.07.045

Veldman, E. R., Jia, Z., Halldin, C., & Svedberg, M. M. (2016b). Amyloid binding properties of curcumin analogues in Alzheimer's disease postmortem brain tissue. *Neuroscience Letters*, *630*, 183–188. https://doi.org/10.1016/j.neulet.2016.07.045

Walsh, S., Merrick, R., Milne, R., & Brayne, C. (2021). Aducanumab for Alzheimer's disease? *BMJ*, n1682. https://doi.org/10.1136/bmj.n1682

Webster, S. J., Bachstetter, A. D., Nelson, P. T., Schmitt, F. A., & van Eldik, L. J. (2014). Using mice to model Alzheimer's dementia: an overview of the clinical disease and the preclinical behavioral changes in 10 mouse models. *Frontiers in Genetics*, *5*. https://doi.org/10.3389/fgene.2014.00088

Yang, F., Lim, G. P., Begum, A. N., Ubeda, O. J., Simmons, M. R., Ambegaokar, S. S., Chen, P. P., Kayed, R., Glabe, C. G., Frautschy, S. A., & Cole, G. M. (2005). Curcumin Inhibits Formation of Amyloid β Oligomers and Fibrils, Binds Plaques, and Reduces Amyloid in Vivo. *Journal of Biological Chemistry*, *280*(7), 5892–5901. https://doi.org/10.1074/jbc.M404751200

Yiannopoulou, K. G., & Papageorgiou, S. G. (2020). Current and Future Treatments in Alzheimer Disease: An Update. *Journal of Central Nervous System Disease*, *12*, 117957352090739. https://doi.org/10.1177/1179573520907397

Zhang, W., Jiao, B., Xiao, T., Liu, X., Liao, X., Xiao, X., Guo, L., Yuan, Z., Yan, X., Tang, B., & Shen, L. (2020). Association of rare variants in neurodegenerative genes with familial Alzheimer's disease. *Annals of Clinical and Translational Neurology*, *7*(10), 1985–1995. https://doi.org/10.1002/acn3.51197

Zheng, K., Dai, X., Xiao, N., Wu, X., Wei, Z., Fang, W., Zhu, Y., Zhang, J., & Chen, X. (2017). Curcumin Ameliorates Memory Decline via Inhibiting BACE1 Expression and β-Amyloid Pathology in 5×FAD Transgenic Mice. *Molecular Neurobiology*, *54*(3), 1967–1977. https://doi.org/10.1007/s12035-016-9802-9

SUPPLEMENTAL MATERIALS

Annex 1

To the vice dean for academic affairs of the Faculty of Science and Technology
Institute of Technology, University of Tartu
Application for establishing restrictions on the publishing of the graduation thesis, and declaring the defense private

Name	Seyedeh Elnaz Sadat Mansouri
Date of birth	26.12.1991
Curriculum	bioengineering
Supervisor	Miriam A. Hickey
Graduation thesis title	A preclinical trial of Bisdemethoxycurcumin in a mouse model of Alzheimer's disease

[X] I request my graduation thesis not to be published until …26.05.2025……(date) for the reason indicated below:

- [ ] Economic copyright rights belong to other people
- [ ] Thesis includes personal data and the data subject has not agreed to publishing
- [ ] State secret
- [ ] Trade secret
- [X] In future, the graduation thesis will be published as a scientific article
- [ ] Other reasons

Explanation (reasons why restrictions are applied for and why for the particular period):

We request that this thesis not be published as this would jeopardise our ability to publish findings in an academic journal.

[ ] I request my defence to be declared private.

Explanation (reasons for declaring the defence private):

Application has the following annexes (to be filled in if there are annexes, i.e. the company's confirmation that the thesis involves a trade secret):
1. Thesis
2.

Date and student's signature 27.05.2022 Seyedeh Elnaz Sadat Mansouri

Date and supervisor's signature

NON-EXCLUSIVE LICENCE TO REPRODUCE THESIS AND MAKE THESIS PUBLIC

I, Seyedeh Elnaz Sadat Mansouri,

1. grant the University of Tartu a free permit (non-exclusive licence) to:

reproduce, for the purpose of preservation, including for adding to the DSpace digital archives until the expiry of the term of copyright, my thesis

A preclinical trial of Bisdemethoxycurcumin in a mouse model of Alzheimer's disease

supervised by Associate Prof. Miriam Hickey,

2. I grant the University of Tartu the permit to make the thesis specified in point 1 available to the public via the web environment of the University of Tartu, including via the DSpace digital archives, under the Creative Commons license CC BY NC ND 4.0, which allows, by giving appropriate credit to the author, to reproduce, distribute the work and communicate it to the public, and prohibits the creation of derivative works and any commercial use of the work from **26.05.2025** until the expiry of the term of copyright,
3. I am aware that the author retains the rights specified in points 1 and 2.

4. I confirm that granting the non-exclusive licence does not infringe other persons' intellectual property rights or rights arising from the personal data protection legislation.

Seyedeh Elnaz Sadat Mansouri
27.05.2022